

**DANISH METEOROLOGICAL INSTITUTE**

**TECHNICAL REPORT**

**01-13**

**Evaluation of the AMIS Gridded Observations and  
Radar derived 24-hour Accumulated Precipitation  
by Comparison with Climate Grid - Denmark  
Gridded Observations**

**March 2001**

**Steffensen M.**

**Vejen F.**

**Hilden A.**

**Overgaard S.**

**Scharling M.**

**Jüngling H.**

**ISSN 0906-897X (print)**

**ISSN 1399-1388 (online)**



**Copenhagen 2001**



## **Preface**

This report presents a comparison of gridded 24-hour accumulated precipitation fields from the DMI Climate grid - Denmark with corresponding DMI AgroMeteorological Information System (AMIS) fields and fields generated from Radar derived precipitation observations. The investigation was carried out at DMI in 2000 as task number 2 “Forbedrede vejrdata til lokal varsling og beslutningsstøtte for behandlingsbehov mod fugtelskende svampe i korn” in the project “Videreudvikling af beslutningsstøttesystemer” in Pesticide Action Plan II commissioned by the Danish Ministry of Environment and Energy and the Ministry of Food, Agriculture and Fisheries.

*DMI, March 2001*

*Michael Steffensen*

*Anna Hilden*

*Flemming Vejen*

*Søren Overgaard*

*Mikael Scharling*

*Helle Jüngling*

## List of contents

1.....	<b>Introduction</b>	3
1.1.....	General	3
1.2.....	Methods and Data	3
1.3.....	Outline	4
1.4.....	Abbreviations	4
1.5.....	Glossary	5
2.....	<b>The Field Types</b>	7
2.1.....	CLIMATE GRID - DENMARK	7
2.2.....	AMIS	8
2.3.....	Radar derived 24-hour Accumulated Precipitation	10
2.3.1.....	Data representation	10
2.3.2.....	Pre-processing	10
2.3.1.....	Estimation of precipitation sums	11
3.....	<b>Evaluation of Cases</b>	13
3.1.....	July 14 <sup>th</sup> , 1998: A Cold Front	13
3.2.....	June 24 <sup>th</sup> , 1999: Showers	17
3.3.....	August 5 <sup>th</sup> , 1999: Anaprop	23
3.3.....	August 19 <sup>th</sup> , 1999: Heavy Precipitation	25
3.4.....	Conclusions	29
4.....	<b>Verification</b>	30
4.1.....	Data	30
4.2.....	Verification Methods	31
4.3.....	Results	31
4.3.1.....	1998	31
4.3.2.....	1999	32
4.4.....	Conclusions	34
5.....	<b>Conclusions and Outlook</b>	35
6.....	<b>References</b>	37

## Appendices

- Appendix A: A brief explanation of errors on weather radar data.
- Appendix B: Tables with the overall statistics for 1998 and 1999
- Appendix C: Contingency tables for AMIS for each month in the growing season 1998
- Appendix D: Contingency tables for AMIS for each month in the growing season 1999
- Appendix E: Contingency tables for radar for each month in the growing season 1998
- Appendix F: Contingency tables for radar for each month in the growing season 1999

# **1. Introduction**

## **1.1 General**

A central component of DMI's AgroMeteorological Information System (AMIS) is the interpolation of observed meteorological data to the 10 by 10 kilometre AMIS grid. As has been documented elsewhere (Hilden and Hansen, 1998), the AMIS observational data are generally of high quality, however the fields of 24-hour accumulated precipitation tend to be too smooth, not reflecting the fine-scale spatial structure of the actual precipitation fields, probably stemming in part from the quite simple, isentropic interpolation scheme used to calculate the data from the raw observed values.

An obvious possibility for improving the AMIS 24-hour accumulated precipitation observational field would be to exploit the fine-scale radar data from DMI's operational weather radars in Kastrup, Rømø and Sindal.

The present study addresses the question of how and to what extent the gridding of observations in AMIS might benefit from a closer connection to radar derived 24-hour accumulated precipitation.

## **1.2 Methods and Data**

The investigation was performed for two growing seasons of six months for which a homogeneous set of archived raw radar data was available: April through September, 1998 and April through September, 1999. Precipitation during the 06:00 to 06:00 UTC (corresponding to 08:00 to 08:00 Danish summertime) constitute the 24-hour accumulated precipitation.

The analysis is restricted to the Jutland area because the characteristics of the Kastrup radar is somewhat different from the characteristics of the radars at Rømø and Sindal. The 24-hour accumulated precipitation for Jutland was therefore derived from data from Rømø and Sindal on a grid corresponding to Climate grid - Denmark .

The data sets compared were:

- Fields of 24-hour accumulated precipitation from Climate grid - Denmark ;
- AMIS observation fields of 24-hour accumulated precipitation;
- Radar derived 24-hour accumulated precipitation from archived data from the radars situated at Rømø and Sindal;

Climate grid - Denmark has a 10 x 10 km grid covering Denmark. The 24-hour accumulated precipitation in each grid cell is interpolated on the basis of data from about 500 manual precipitation stations. The data has undergone a thorough quality check before the interpolation, but are not corrected for possible influence from wind, wetting or evaporation, which comply with the operational precipitation data in AMIS.

The data are available with approximately a month delay and can as such not be part of a real-time operational system.

Climate Grid - Denmark is at present our best measure of accumulated precipitation and is therefore selected as the “true” values of 24-hour accumulated precipitation. The climate grid - Denmark is further described in chapter 2.1.

The AMIS observational field is a 10 x 10 km<sup>2</sup> grid covering Denmark. The AMIS grid data are interpolated from about 70 standard meteorological observations made at SYNOP stations in Denmark, southern Sweden and Germany. The squares in the AMIS fields are assumed to be identical to the squares in Climate grid - Denmark, which is only partly true but with negligible differences for this study. The AMIS system is further described in chapter 2.2.

The radar derived accumulated precipitation is compiled from several radar echo images from the radars at Rømø and Sindal. The radar derived accumulated precipitation has a 2 x 2 km<sup>2</sup> grid resolution. This has been resampled to a 10 x 10 km<sup>2</sup> grid resolution. The resampling reduces information in the radar data but is done in order to fit the climate grid - Denmark grid. The radar derived precipitation is further described in chapter 2.3.

The evaluation was done for each AMIS square and each day on monthly samples using standard meteorological verification measures. In addition to the statistical verification, a qualitative validation was carried out for three days with different characteristic weather types or radar echoes.

### **1.3 Outline**

The report is organised as follows:

Chapter 2 contains brief descriptions of the three different fields: Climate grid - Denmark , the AMIS field, and the radar derived 24-hour accumulated precipitation. Chapter 3 and Chapter 4 present the results of the qualitative case studies and the statistical verification, respectively. In Chapter 5 some central conclusions are drawn, and a look is taken at the possible directions of future work on integration of radar derived precipitation into the AMIS system. References are given in Chapter 6.

Detailed results of the statistical verification are compiled in an Appendix B to F.

A list of abbreviations and acronyms used throughout the report is given below.

### **1.4 Abbreviations**

Climate grid - Denmark    Climate grid - Denmark , see Chapter 2.1.

AMIS                    AgroMeteorological Information System, see Chapter 2.2 AMIS.

RADAR                Radar derived 24-hour accumulated precipitation, see Chapter 2.3.

ME	Mean Error, i.e. the sum of the difference between the analysed values and the observations, divided by the number of observations.
MAE	Mean Absolute Error, i.e. the sum of the absolute difference between the analysed values and the observations, divided by the number of observations.
RMSE	Root Mean Square Error, i.e. square root of the mean squared error.
HR	Hit Rate, The sum over each precipitation category of number of correct estimate (AMIS or Radar ) of this category divided by the total number of occurrence in Climate Grid of this category.
HKSI	Hanssen-Kuipers' skill index with climate as reference. HKSI is 1 for a perfect forecasting system and 0 for a "no skill" system. Negative values of HKSI indicates that the forecasting system is inferior to the reference. (Hanssen, A.W., and W.J.A. Kuipers, 1965)

All Hit Rates are given as fractions.

ME, MAE and RMSE are in mm/24hr in tables showing statistics.

## 1.5 Glossary

Anaprop:	In meteorological situations associated with nonstandard refraction, strong downward bending of the radar beam may occur leading to echoes from ground targets even far from the radar. This cause spurious echoes. Nonstandard refraction occur when the vertical distributions of temperature and specific humidity are other than normal.
Attenuation:	The beam power is attenuated due to atmospheric gasses and hydrometeors, i.e. clouds, rain, snow and hail.
Beam filling:	The received power corresponds to the backscattering from a volume of air. If the beam volume is not uniform filled with hydrometeors, e.g. in case of partially filling, representativity problems may arise. The cross section of a radar beam increases with increasing range, thus the problem increases with range.
Beam power profile:	The power profile is the energy level in the beam across the beam axis.
Bright band:	The bright band is the layer in which melting of snow is going on causing a higher reflectivity than in the layers below and above. A thin coating of water results in a very large increase in the reflectivity of a snow sphere due to a larger backscattering cross section.
Clutter:	The reflection of the radar beam from non-meteorological targets.

- Overshooting: The radar beam is situated above the precipitation layer.
- Reflectivity factor: The volumetric integration of the drop diameter in sixth power in the unit  $\text{mm}^6\text{mm}^{-3}$ .
- Refraction: The air-mass properties, i.e. temperature, pressure and humidity, are sufficiently variable to produce small changes in the speed of propagation. This may lead to refraction of the radar ray and produce marked changes in the direction of propagation.
- Sidelobe: The energy is concentrated into a beam along the radar parabolas axis which is known as the major lobe. Smaller secondary lobes, the sidelobes, are usually found with their central axis directed at various angles with the parabolas axis.

## 2. The Field Types

### 2.1 CLIMATE GRID - DENMARK

For the purpose of producing high quality grid data a program for optimizing the quality check of meteorological data has been developed as well as a routine which can handle interpolation of data from spatially pure located weather stations. The results of the interpolations are referred to as climate grid - Denmark. (DMI Technical report 99-12 and 15)

Denmark has about 70 weather stations which measure temperature, wind and relative humidity. A quarter of the stations measure global radiation. In addition to the weather stations there are about 500 manual precipitation stations. The figure below shows the manual precipitation stations net (1999) and the 10x10 km grid cells covering Denmark.

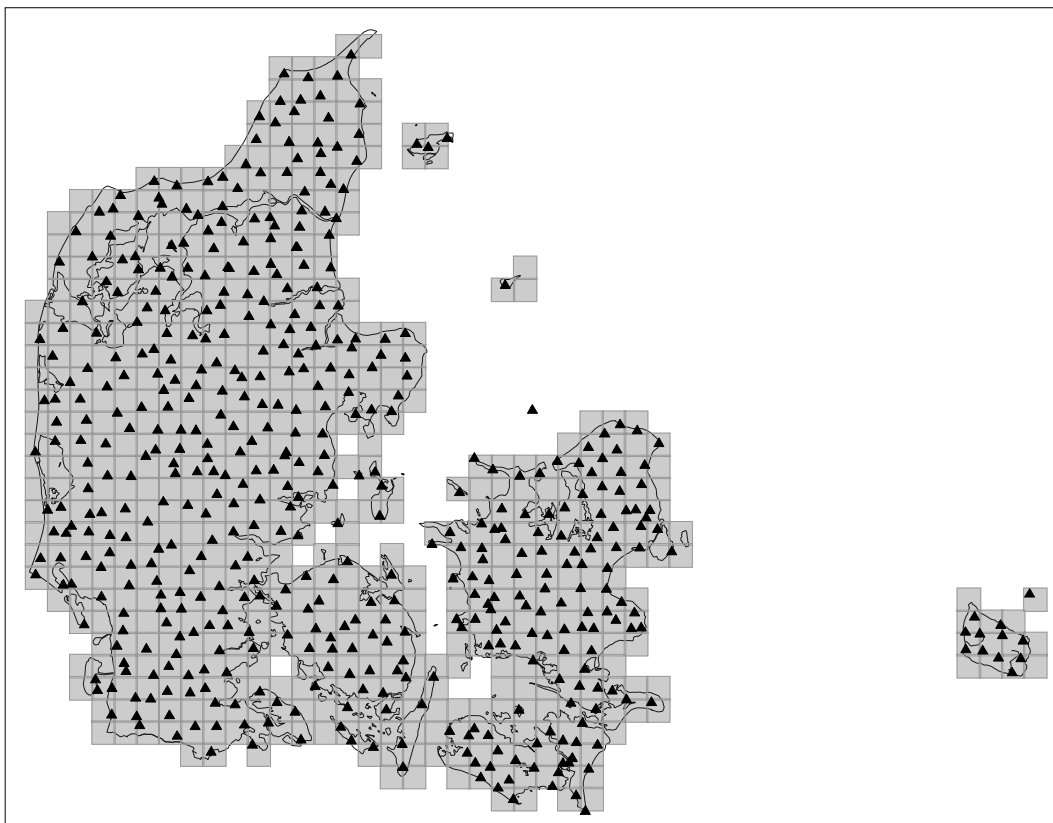


Figure 2.1: Precipitation station net year 1999 (black) and 10x10 km grid cells (gray).

Generally, the single most important factor with the greatest impact on the local climate in Denmark is the distance to the sea. Consequently, an uneven station coverage constitutes a problem in connection with a classical interpolation, because areas with poor coverage may risk being affected by remote stations which are climatically very different from the climate prevailing at the interpolation point.

In climate grid - Denmark the interpolation problem described above has been attempted to be offset by carrying out two interpolations – one involving near-coast stations and one involving inland stations. The importance of the two interpolation results is then weighted for each interpolation point on the basis of the distance to the ocean. This method has been used when calculating temperature, humidity and wind grid values. Interpolating global radiation is performed by a single calculation as there are not enough stations measuring this parameter to divide them into an inland and a near-coast group. Contrary to the weather stations the density of manual precipitation stations is very high and at the same time geographically even located, and a double interpolation is therefore not necessary. The algorithm which is used for interpolation is inverse-distance. To reduce calculation time, only points over land areas are calculated<sup>1</sup>. The interpolation points are subsequently aggregated into rectangular grid cells<sup>2</sup>, so that the values obtained represent the area inside the grid cell.

Potential evapotranspiration is calculated using grid values as input to a modified Penman formula (Mikkelsen, H.E. & Olesen J.E 1991).

Monthly and yearly values are calculated on the basis of the interpolated point values so that any rounding errors are minimized.

## 2.2 AMIS

AMIS, DMI's AgroMeteorological Information System, provide farmers and other users within the Danish agricultural community with local meteorological data on a real-time basis. All numerical data are available on a 10 by 10 kilometre grid covering Danish land area. There are 632 AMIS points, or 'squares', in all (Figure 2.2).

The AMIS observational data are computed from standard meteorological observations made at SYNOP stations in Denmark, southern Sweden and northern Germany, and at Danish automatic climate stations. For each AMIS square, the value of a given parameter at a given time is obtained by interpolation of the values from stations within a predefined cutoff radius. The interpolation algorithm is simple distance weighting with weights proportional to  $d^r$ , where  $d$  is distance and  $r$  is a parameter dependent (negative) power. In the rare case of very poor data coverage, all available measured values from stations near Denmark are used. Certain stations known to have a bad impact on the AMIS fields for one or more parameters are left out in the interpolation for these parameters.

Table 2.1 gives an overview of the observational parameters which were included in AMIS in the growing season of 1999. The approximate number of measuring stations contributing to the AMIS fields for each parameter and the interpolation power and cutoff radius are also given.

---

<sup>1</sup> Temperature, humidity, wind and global radiation is calculated at intervals of 10 km and precipitation at intervals of 5 km.

<sup>2</sup> 20\*20 and 40\*40 km for temperature, humidity, wind and global radiation. 10\*10, 20\*20 and 40\*40 km for precipitation.

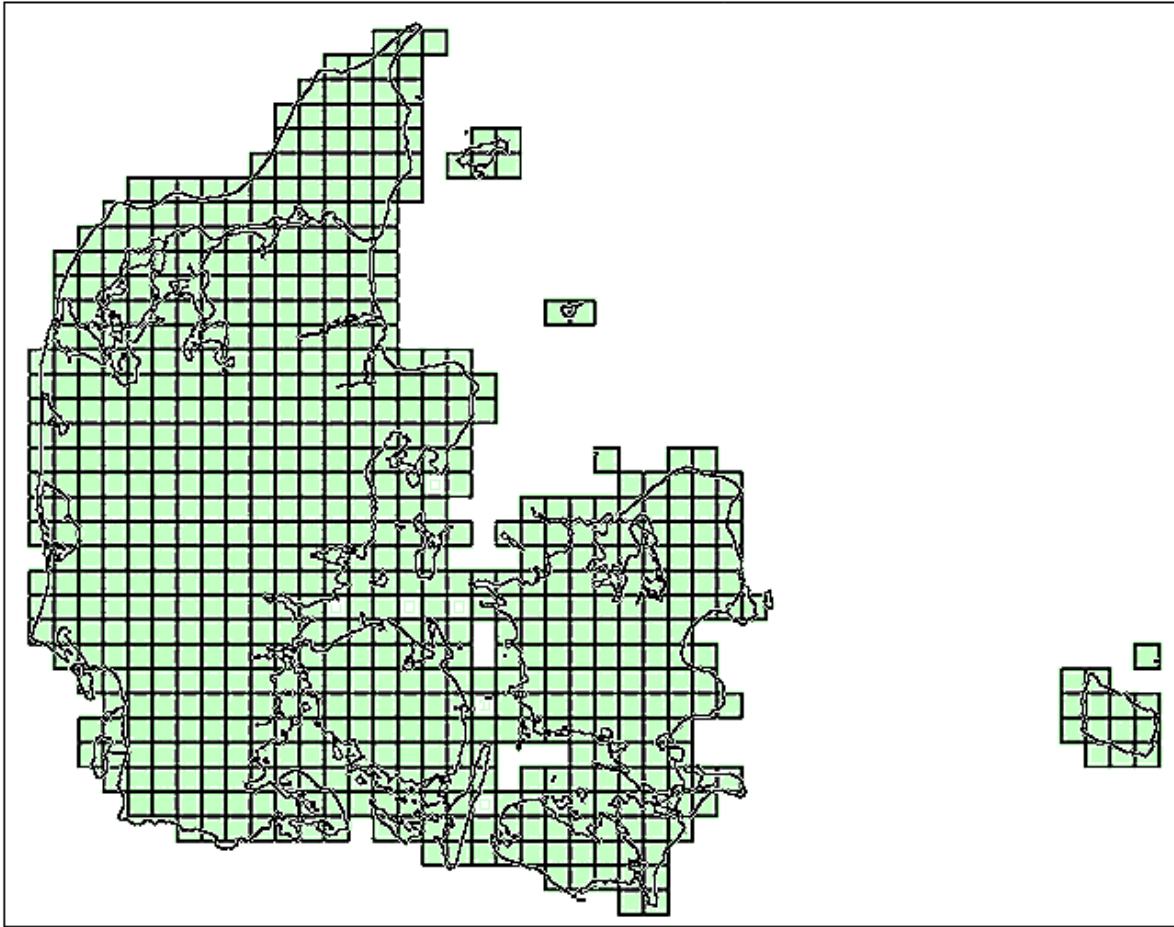


Figure 2.2 The AMIS grid

Parameter	Time	No. of stations (approx.)	Interpol. Radius (km)	Interpol. Power	Description
<b>2MT</b>	00,03,...,21 UTC	150	60	-1.7	Temperature 2 m above ground (degrees Celsius)
<b>2MRH</b>	00,03,...,21 UTC	150	60	-1.7	Relative humidity 2 m above ground (percent)
<b>10MFF</b>	00,03,...,21 UTC	150	70	-1.3	Wind speed 10 m above ground (m/s)
<b>24HAT</b>	06-06 UTC	113	80	-1.4	24 hours' accumulated precipitation (mm)
<b>24HPEV</b>	06-06 UTC	38	80	-1.4	24 hours' accumulated potential evaporation (mm)
<b>24HGLR</b>	06-06 UTC	19	100	-2.3	24 hours' accumulated radiation ( MJ/m <sup>2</sup> )

Table 2.1 AMIS observed parameters

## **2.3 Radar derived 24-hour Accumulated Precipitation**

### **2.3.1 Data representation**

The Sindal and Rømø radars are conventional C-band radars. They scan every 10 minute at several beam elevations, and the sampling rate of a scanline at a given elevation and azimuth is 450 kHz corresponding to 333 m range bins. One pseudo-CAPPI-level and eleven CAPPI-level images (Constant Altitude Plan Position Indicator) are produced from the full data volume. Each CAPPI-level represents a one km thick horizontal layer made by interpolation between the elevation scan data from which vertical reflectivity profiles can be made. The pseudo-CAPPI-level image is made from the lowest elevation beam. Each image comprises of 240×240 pixels each representing an air volume of the size 2×2×1 km<sup>3</sup>, 2 km horizontally and 1 km vertically. The radar range is 240 km. The radar receiver has been designed with wide dynamic range to enable rain intensity measurement from about 0.01 to 1000 mm/hr. The reflectivity is measured in count units from which the reflectivity factor  $Z$ , and in turn the rain rate  $R$ , is calculated.

### **2.3.2 Pre-processing**

The radar calibration system operates on at-site Polar radar data, and various corrections are applied to data during pre-processing at the radar site.

Corrections are made for loss of effects in the radar system. Correction for beam power losses at range ( $r^2$  correction) are done in order to establish range independent measurements and to account for the loss of power during propagation of the beam through the atmosphere. Correction for the attenuation due to gasses is small compared to that caused by hydrometeors, but attenuation, particularly in heavy rainfall and when a bright band is present, may be substantial. Beamshape losses are accounted for by integration in azimuth over one antenna beam width. Correction for attenuation due to the atmosphere and hydrometeors are done by the so-called en-route correction. A clutter map is used to subtract echoes from polar pixels which are persistently affected by clutter, and by histogram analyses some of the strongest false echoes arising from non-precipitating targets are removed. The Polar data are then converted to Cartesian grid representation by spatial interpolation, a irreversible process by which loss of information can be extensive at long ranges.

After receipt of data a fixed threshold filter is applied to the radar image to remove reflectivities too weak to be precipitation of any importance, perhaps the simplest segmentation method. It is assumed that the objects have pixel values generally different from the background. A threshold value for non-precipitation has been defined using a relationship between reflectivity and rain rate, and probably no precipitation pixels are removed from the radar image.

Strong echoes from non-precipitating targets will persist in the image as artificial precipitation unless something is done. Much of this clutter is suppressed by analysing vertical reflectivity profiles. All pixels in the radar image coincident with pixels having no

echo at the level just above is reset to zero. The method uses the fact, that precipitation systems most often extend well above ground surface. Problems may arise for drizzle and for snow showers during winter having echo tops at relatively low level.

A special median filter is used to remove residual clutter; it replaces a pixel value by the median of its neighbours. A median filter is one of the better edge preserving smoothing filters and it has shown to be sufficient in most cases. The method works well if clutter occurs amongst widespread low intensity rainfall, or in dry conditions. Detection of clutter is more difficult if small scale convective precipitation is present in the image, e.g. as very small isolated showers and pixels partially filled with small convective cells, and they may be removed. In case of strong anomalous propagation of the radar beam (anaprop) false echoes will remain in the image and appear as precipitation. Anaprop is normally very extensive and it may affect all elevation beams deleteriously.

The most serious of all errors on radar data is the bright-band effect, that is caused by enhanced reflection from melting snow crystals just beneath the 0°C isotherm. It can cause large errors in estimated radar rain rates. Bright-bands are commonly present in Denmark during the winter season. Correction for it must be done during pre-processing, otherwise rain gauge adjustment may become very unreliable. The reason is among others, that the magnitude of the bright-band error is a function of the reflectivity enhancement caused by the bright-band as well as the height and thickness of the bright-band relative to the elevation and width of the radar beam. In the present study, the bright-band is ignored because it is assumed unimportant in the growth season, except in the beginning of the season, especially in early April, where it may be present in the images. Furthermore, in the growth season the bright-band is most often prevailing at higher levels and is not found in the pseudo-CAPPI image relatively close to the radar.

Due to the curvature of Earth the radar beam rises above ground level at increasing range, the measurements are made at higher altitudes, and the reflectivity decrease with range due to increasing beam elevation which makes the reflectivity measurements unrepresentative of the surface precipitation. Because the lowest beam elevation is 0.5° and the highest is well below vertical, low level targets at range and above the radar are not detected at all. An often observed range effect is beam overshooting. Range adjustments are not applied to improve the radar performance at long range.

### **2.3.1 Estimation of precipitation sums**

The energy reflected from hydrometeors in a volume of air depends on the diameter  $D$  in sixth power and the number of particles  $N$ . The reflectivity factor  $Z$ , which is calculated from the returned power, is related to precipitation intensity  $R$  (mm/hr) by relationships of the general form  $Z=AR^b$ , where  $A$  and  $b$  are empirical constants (e.g. see Battan, 1973). Basically, the relation between  $R$  and  $Z$  depends on the dropsize distribution in a unit volume, thus  $Z$  depends on the precipitation type. Knowing that the value of  $Z$  is proportional to the number of drops in first power but the drop diameter  $D$  in sixth power, the reflectivity factor  $Z$  reaches, for the same rain rate, the largest values in convective precipitation and the smallest

in drizzle because the number of large drops is much larger in convective precipitation than in drizzle.

In this study the so-called Marshall and Palmer (1948) for various types of rain has been used to estimate rain rates. The 24 hours amount of rain  $R_{24}$  is estimated by adjusting every radar image (pseudo-CAPPI image) into rain rate, and then integrating the 10-minute R values pixel by pixel i:

$$R_{24} = \sum_{i=1}^N \left( \frac{Z_i}{A} \right)^{\frac{1}{b}}$$

where  $A=220$ ,  $b=1.60$  and  $N$ =the number of images. Finally,  $10 \times 10 \text{ km}^2$  grid cells are estimated on the basis of the 24 hours precipitation sum image.

### 3. Evaluation of Cases

#### 3.1 July 14<sup>th</sup>, 1998: A Cold Front

The synoptic development over Denmark this day is dominated by a low which enters Jutland near Thyborøn and moves eastwards across northern Jutland and Kattegat towards Sweden. During the morning the wind in Jutland is mainly from south to southwest with light showers in the western and southern parts and in Djursland. Strong to heavy showers are reported from Ringkøbing along the west coast to Thisted airport. Light continuous rain in the most southern part of Jutland. A cold front associated with the low reaches Jutland and is at 12:00 UTC stretching from around Mors in the Limfjord southeast across Funen. The synoptic weather map and the position of the cold front at 12:00 UTC are shown in figure 3.1. The wind behind the front is more westerly and light showers prevail across Jutland with still some strong showers on the west coast. At 15:00 UTC the front has moved further

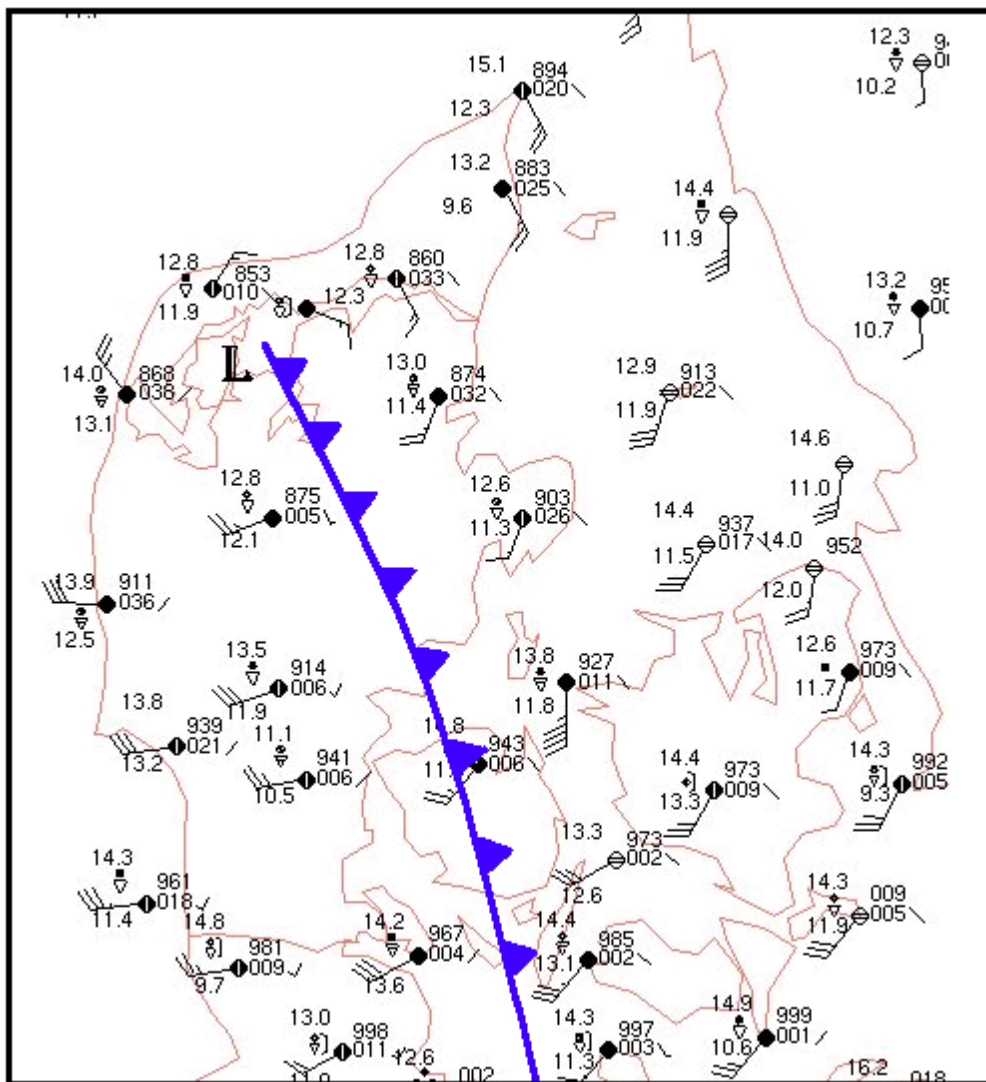


Figure 3.1. Synoptic map for July 14<sup>th</sup>, 1998, 12 UTC.

eastwards to Kattegat and Sealand, though some light widespread showers are still present in Jutland.

Figure 3.2 shows the precipitation contours (red curves) for the radar derived field together with the contours (blue) of the verifying Climate Grid - Denmark and a scattergram in the lower left corner.

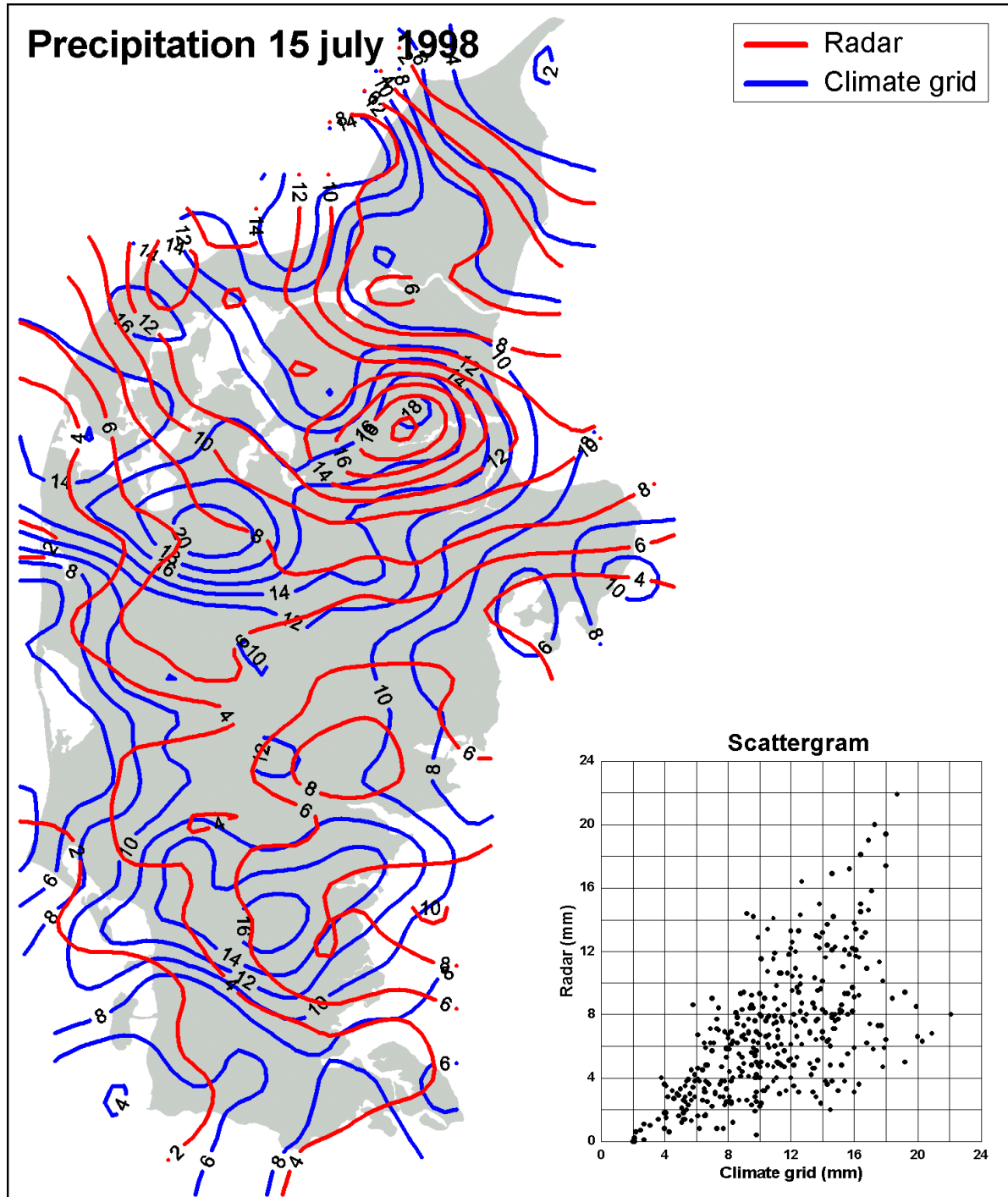


Figure 3.2. Map of precipitation using Radar for July 15<sup>th</sup>, 1998, 12 UTC, and a scattergram to show the accuracy.

The grid precipitation from Climate Grid - Denmark shows up to 15-20 mm of rain at the most wet places. The precipitation pattern was irregular. Generally, the amount of precipitation was underestimated by the two radars according to the scattergram.

This is not surprising because a standard adjustment has been used to transform reflectivity into rain rate, the so-called Marshall-Palmer equation (Marshall and Palmer, 1948) which is valid for not convective frontal rain. The diagram in figure 3.3 shows formulas commonly used for adjustment of drizzle, frontal rain and showers. It is seen, that using a frontal equation on rain shower will result in underestimation of precipitation amount. Thus the standard calibration has to be replaced with an adjustment based on parallel rain gauge recordings.

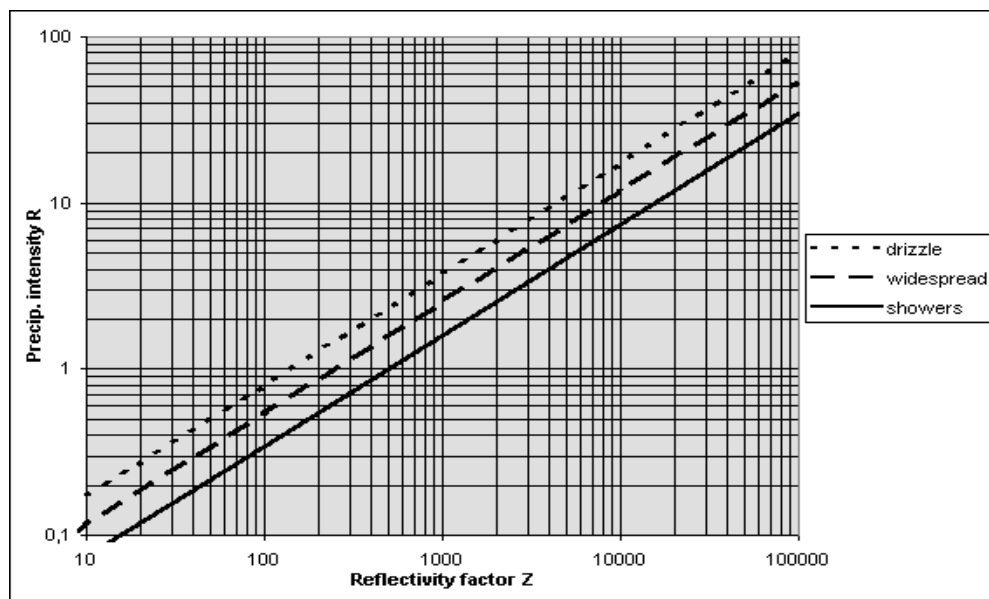


Figure 3.3. A plot of rain rate  $R$  versus reflectivity factor  $Z$  for drizzle  $Z=140R^{1.5}$ , widespread rain  $Z=250R^{1.5}$ , and showers  $Z=500R^{1.5}$  (Battan, 1973). The formula for various types of rain used in this study, the Marshall-Palmer equation, is  $Z=220R^{1.60}$  (Marshall and Palmer, 1948).

The Sindal radar grid agree quite well with the climate grid up to about 100 km range. For example, it is excellent in showing the precipitation maximum of about 18 mm approximately 100 km south of the radar, both concerning amount and position of the maximum. At larger ranges the radar obviously underestimates the precipitation amount, especially as regards the specific maximum in the southern part of the image of about 20 mm. The precipitation pattern has been retrieved quite well.

The Rømø radar has bigger problems than the Sindal radar in showing the amount and spatial distribution of precipitation. In this case, it could not locate the exact position of the areas getting the most precipitation, but on the other hand, it did show the overall precipitation pattern within 100 km range. The precipitation amount was generally underestimated. This is presumably due to an error in the calibration of receiver sensibility that subsequently has been diagnosed.

The Rømø radar has the same problems as Sindal as to see the precipitation maximum in the intersection area of the two radars. This can be seen in the radar images from 14 Juli 1999 at

12UTC where it can be seen that the precipitation echoes are becoming weaker at the larger ranges. In the overlap areas, the two radars are seeing almost the same distribution of precipitation but the rain rate is different (figure 3.4).

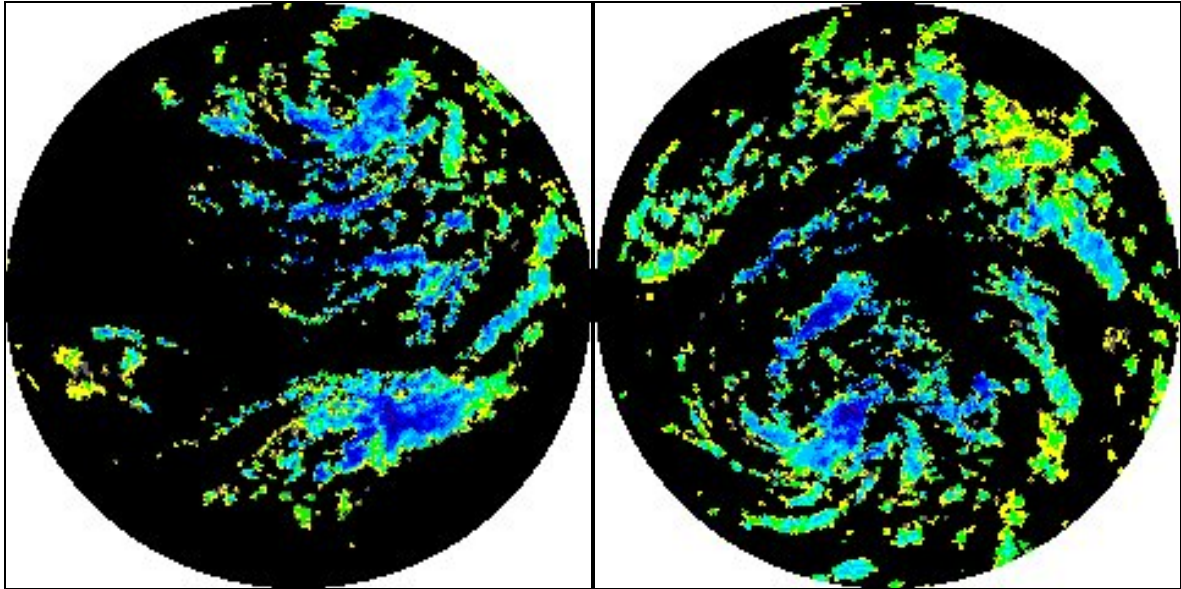


Figure 3.4. Rømø (left) and Sindal (right) images on 14 July 1998 at 12UTC. Dark blue indicates the heaviest rain, yellow and grey is the weakest.

Generally, a weather radar has problems in detecting precipitation at ranges larger than about 100-150 km. A rule of thumb is that closer than 100-150 km radar data can be used quantitatively, but at large ranges it can most often only be used qualitatively unless data is corrected for range related sources of error which can improve results to a certain extent. In radar grid cells at larger ranges were skipped in the comparison better results, e.g. less scatter between climate and radar grids, would be obtained.

The AMIS results in the diagram in figure 3.5 shows a significantly larger scatter, and the radar are of no doubt giving better estimates. There are potentials of even better results because radar data have been processed in the simplest possible way in this pilot study.

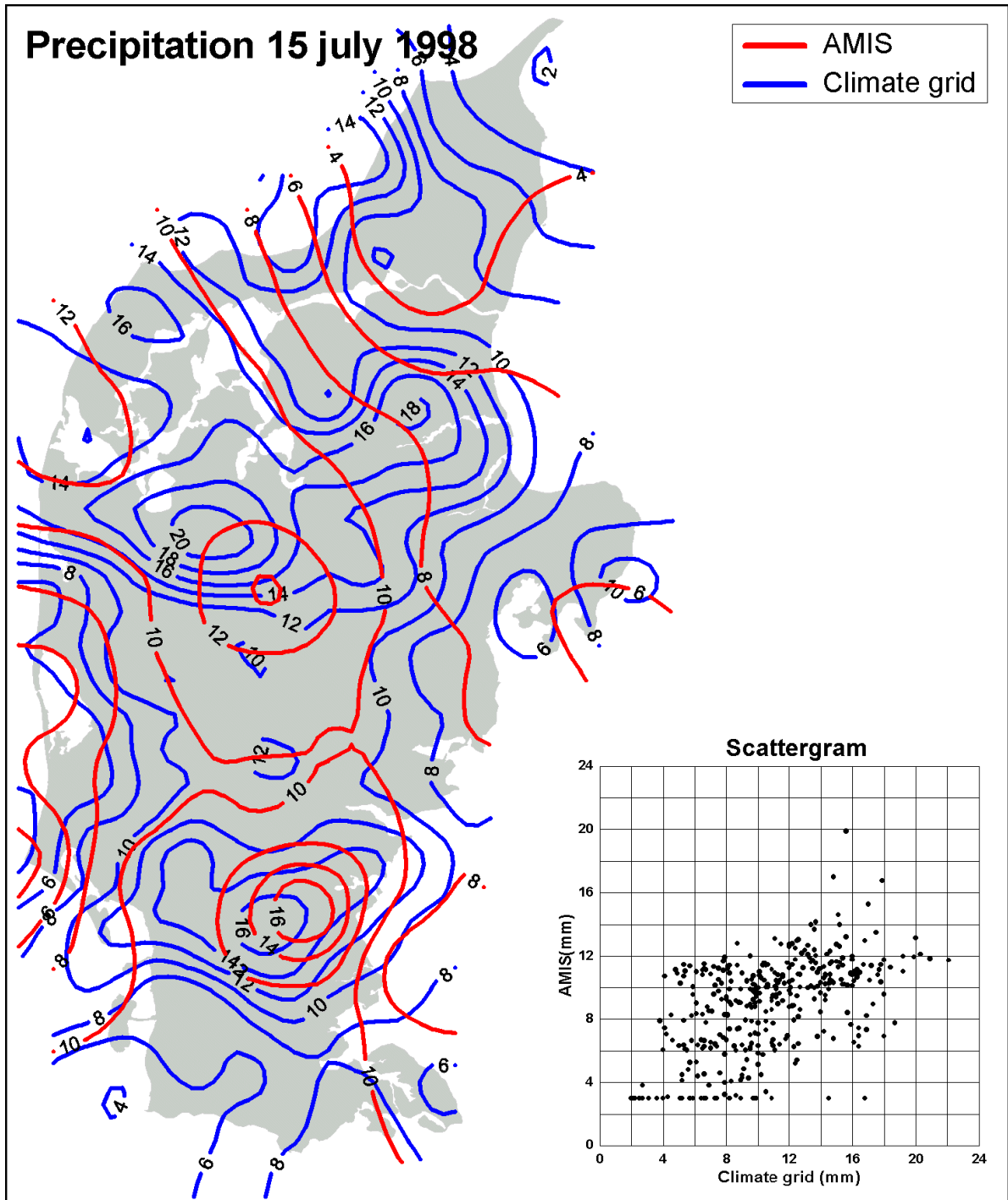


Figure 3.5. Map of precipitation using AMIS for July 15<sup>th</sup> 1998, 12 UTC, and a scattergram to show the accuracy.

### 3.2 June 24<sup>th</sup>, 1999: Showers

The synoptic situation 12 UTC shown in figure 3.6 is dominated by a high pressure area with more than 1020 hPa and a southeast gradient with wind from northwest. This was the general situation during both 24-25 June 1999. Local showers fell mainly in the two areas seen in figure 3.7 showing the precipitation contours (red curves) for the radar derived field

together with the contours (blue) of the verifying Climate Grid - Denmark and again a scattergram in the lower left corner.

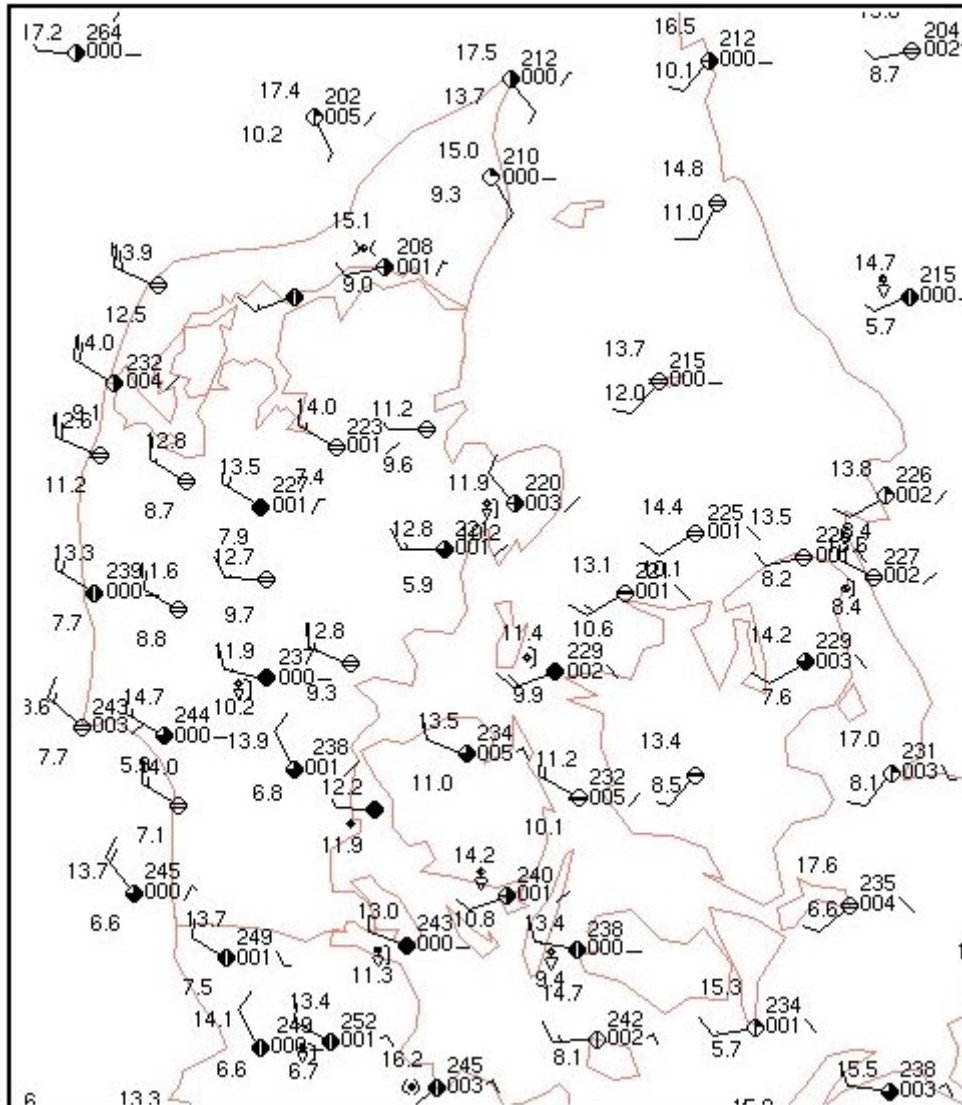


Figure 3.6. Synoptic map for June, 24<sup>th</sup> 1999, 12 UTC.

The northern showers were detected by the Sindal radar and the southern ones by the Rømø radar. Of no doubt the two radars did, in particular, detect the position of the showers precisely as seen in the examples of single Sindal and Rømø radar images in figure 3.8. For example, notice the oblique orientated shower somewhat south of the Sindal radar which is just seen in the north-eastern most edge of the coverage of the Rømø radar. This shower is a good example of what happens at large ranges. The radar is seeing the distribution of the precipitation quite well, but the amount is poorly determined. The shower is situated much closer to the Sindal radar, and the estimation of rain rate is much better indicated by this one than by the Rømø radar.

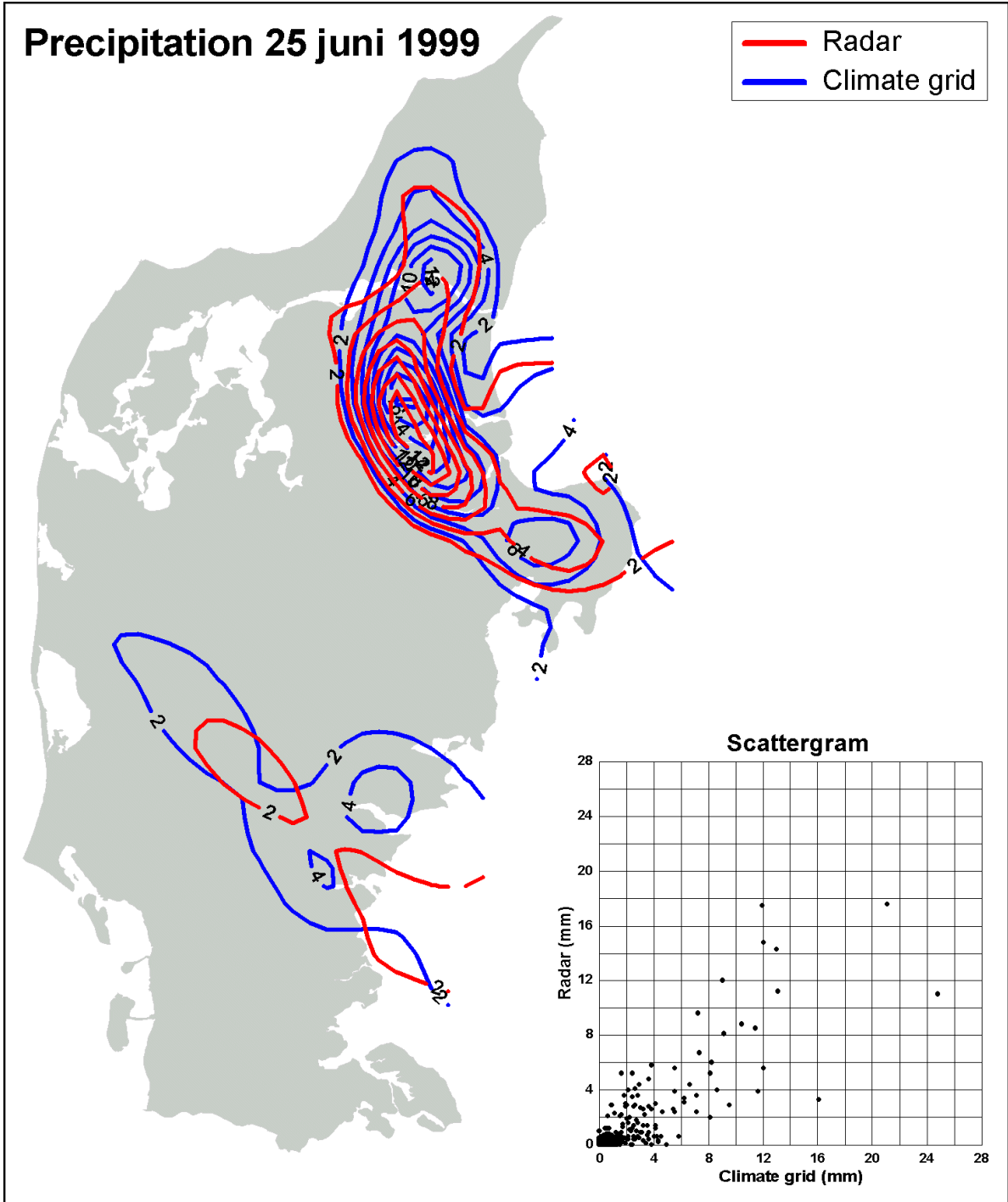


Figure 3.7. Map of precipitation using RADAR for June 25<sup>th</sup> 1999, 12 UTC, and a scattergram to show the accuracy.

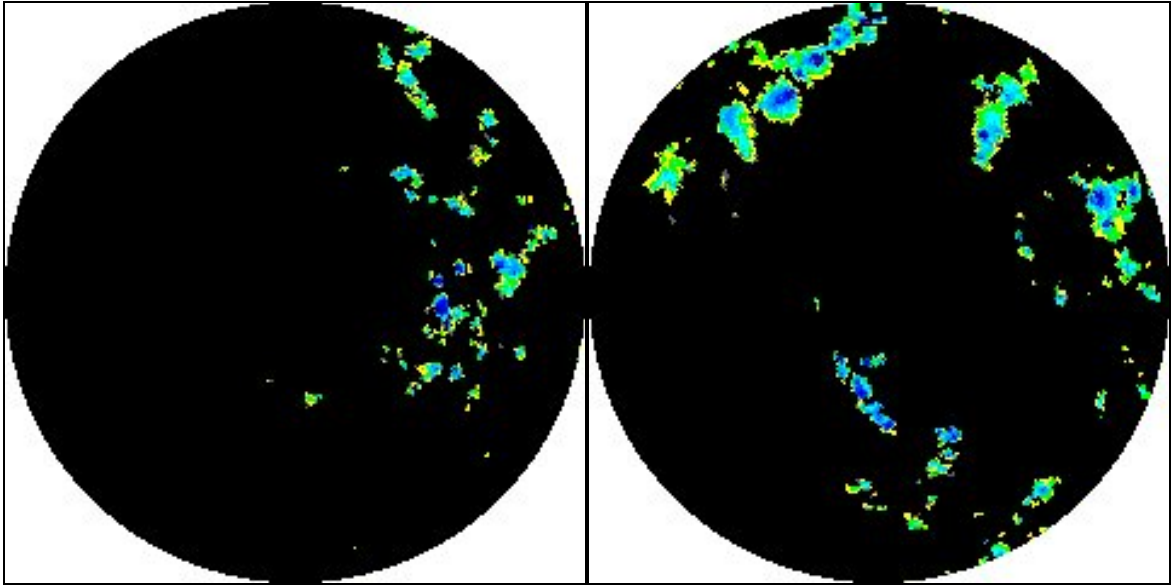


Figure 3.8. Rømø (left) and Sindal (right) radar images on June 24<sup>th</sup> 1999 at 15 UTC. Dark blue indicates the heaviest rain, yellow and grey is the weakest.

Compared with the AMIS result shown in figure 3.10, the radar hits the distribution of precipitation very well, especially concerning no-rain areas (see figure 3.9), but the precipitation amount determined by the radar are quite scattered compared to the climate grid as seen in the diagram in figure 3.7. Especially, this is the case for small precipitation amounts. On the other hand it is promising, that the radar comes up with much better results than AMIS. It has to be noted, that the points in the scatter diagram for the radar includes all grid cells, also those situated at large ranges far away from the recommended distance for quantitative calculations. Probably, a lot of the points with low radar amount can be ascribed to this fact.

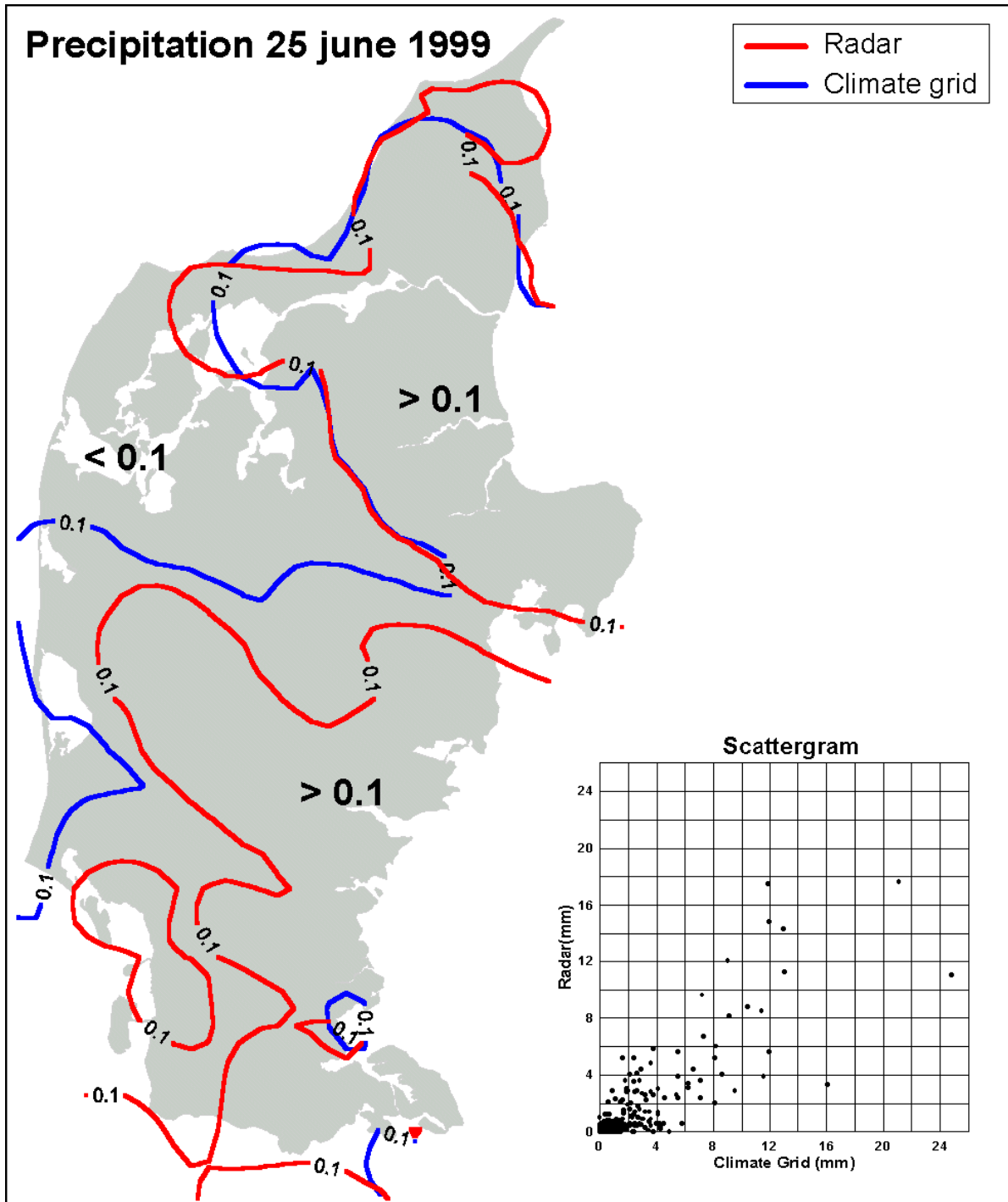


Figure 3.9. Map showing the extent of precipitation using RADAR for July 25<sup>th</sup> 1999, 12 UTC  $<0.1$  refers to no precipitation and  $>0.1$  refers to areas with precipitation.

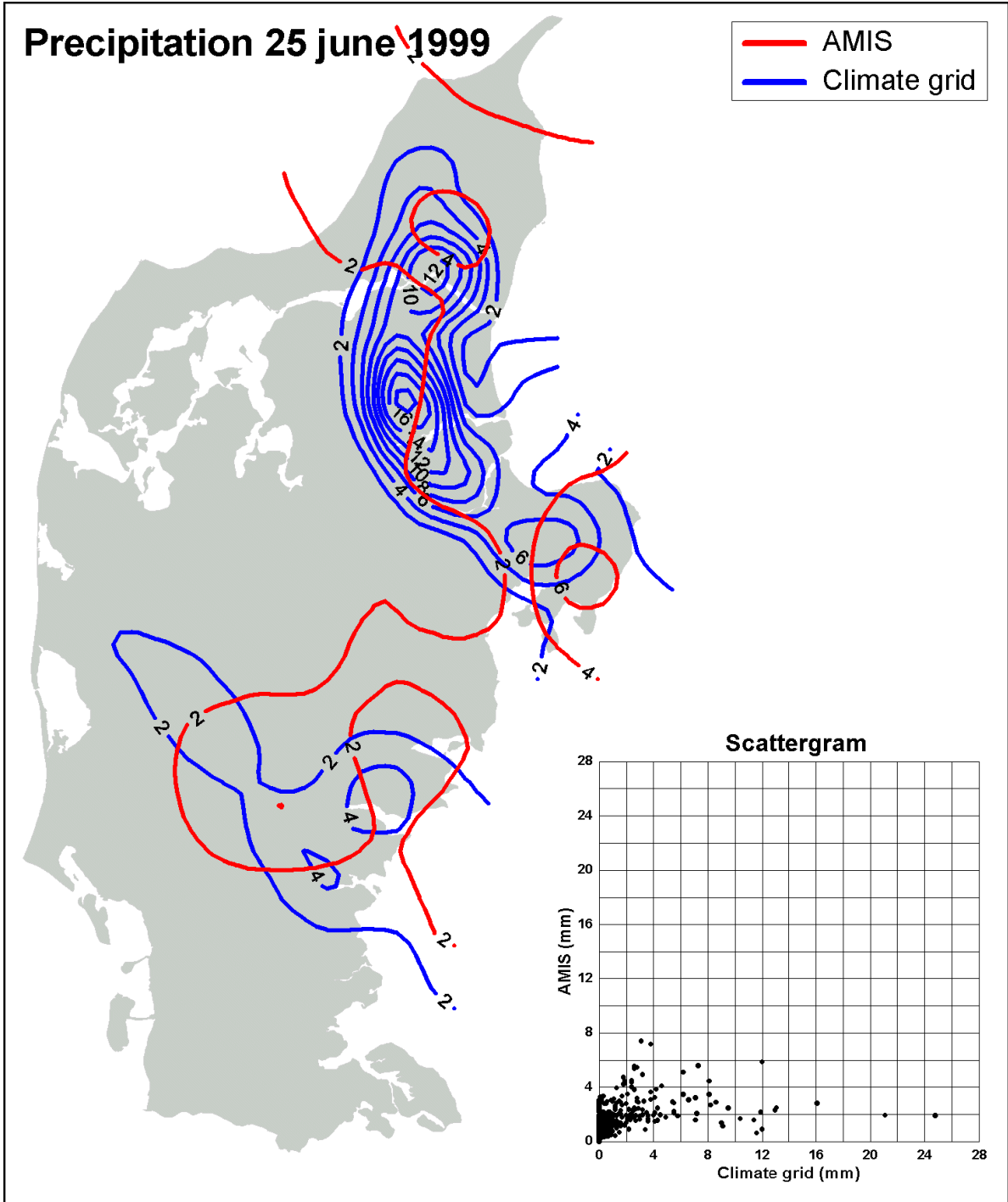


Figure 3.10. Map of precipitation using AMIS for June 25<sup>th</sup> 1999, 12 UTC, and a scattergram to show the accuracy.

### 3.3 August 5<sup>th</sup>, 1999: Anaprop

The weather conditions on this day are very interesting, and the situation differs from the other cases by having no precipitation at all. The atmosphere was stable and there was an temperature inversion, which typically results in anomalous propagation of the radar beam (anaprop). Figure 3.11 shows the

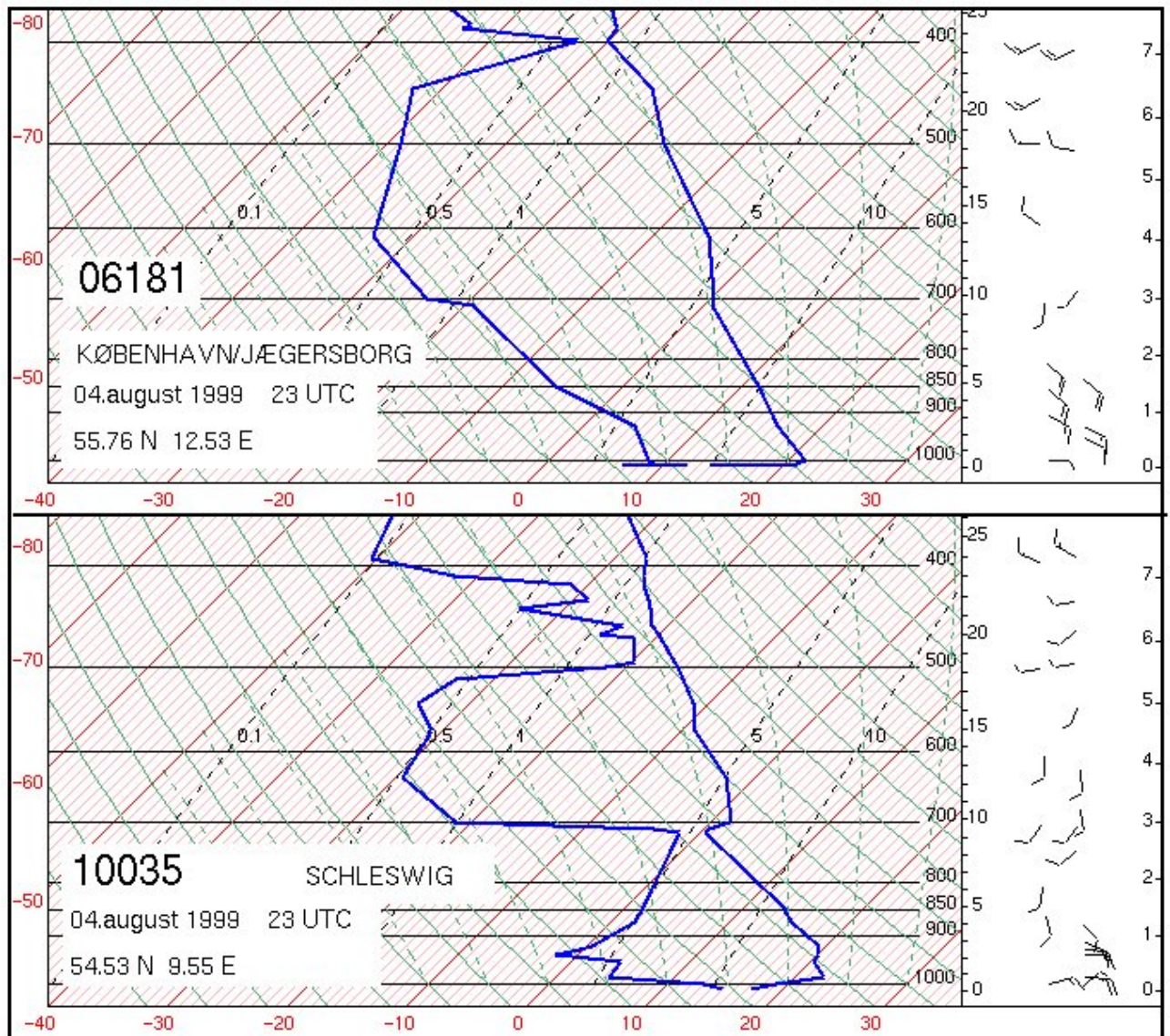


Figure 3.11. Radiosoundings from København/Jægersborg and Schleswig on August 4<sup>th</sup> 1999 at 23 UTC.

radiosoundings from København/Jægersborg and Schleswig at 23 UTC August 4<sup>th</sup>. The temperature inversion at the surface is clearly seen.

The radar beam is refracted more than the curvature of Earth and it hits targets on the ground randomly at nearly all ranges. The result is artificial radar precipitation amounts unless correction for this effect is applied. This has not been done during pre-processing of images in the present pilot project. Methods exist for dampening or removal of anaprop, but this

requires careful filtering of the images, especially because anaprop and precipitation may appear in the same image.

Figure 3.12 shows severe anaprop in a Sindal image on August 5<sup>th</sup> 1999 at 6 UTC. The effect of the terrain is clearly seen as marked echoes from the coastal areas of Southern Norway, Sweden, Zealand and Jutland.

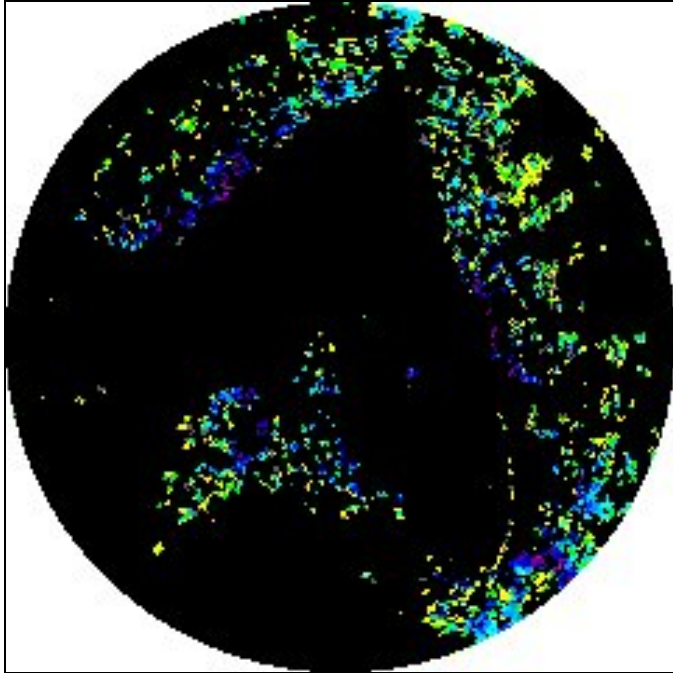


Figure 3.12. A Sindal radar image with marked heavy anaprop, i.e. radar echoes not corresponding to precipitation, on August 5<sup>th</sup> 1999 at 6 UTC. Especially, the coastal areas of Jutland, Zealand, Sweden and Southern Norway is clearly seen.

Figure 3.13 below shows the radar derived accumulated precipitation on this dry day. Not surprisingly, AMIS comes up with the best results for this particular case. However, it is possible to treat radar data in such cases much better to give definitely improved and unambiguously estimates of precipitation sums.

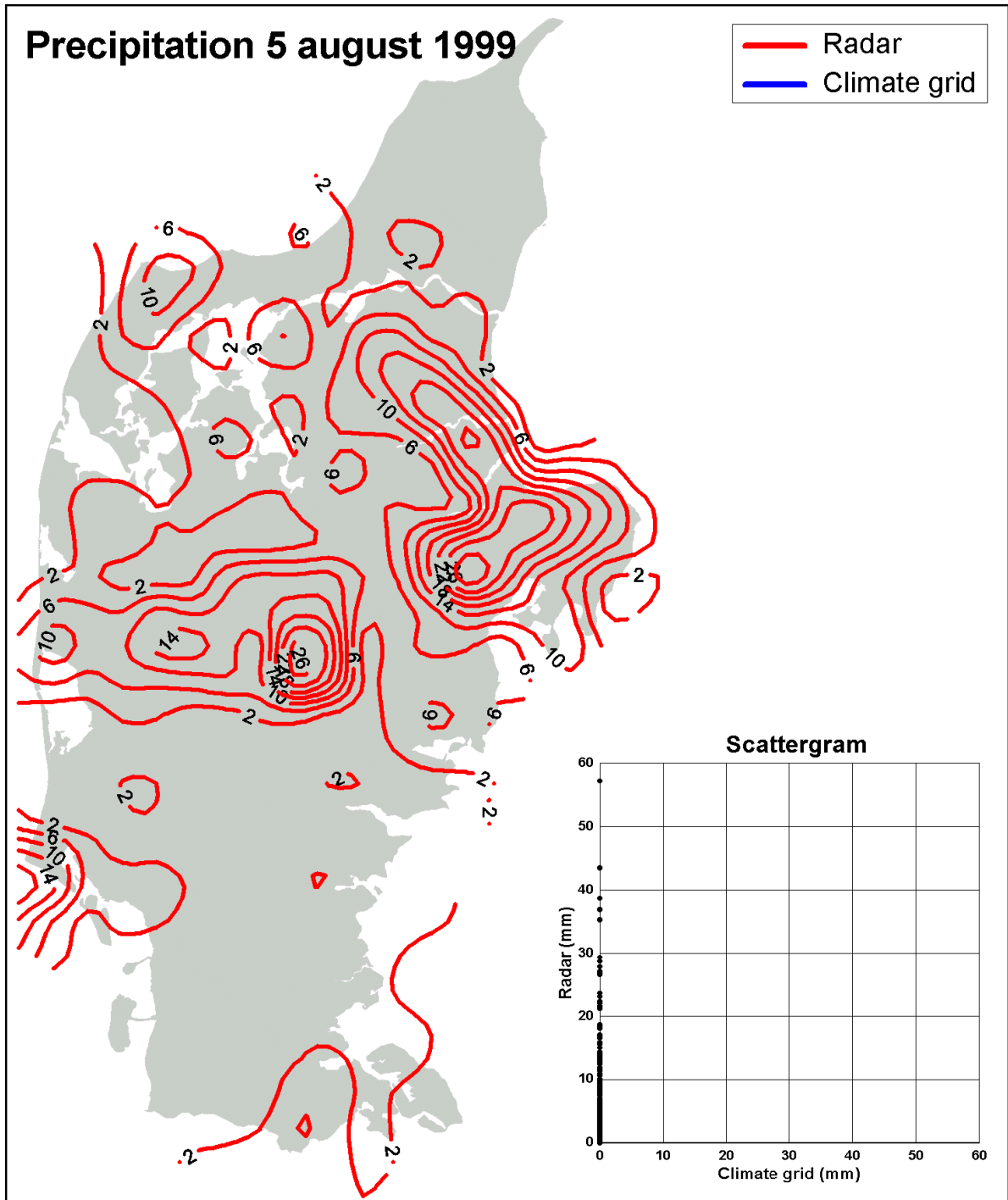


Figure 3.13. Typical map of precipitation using RADAR for August 5<sup>th</sup> 1999, 12 UTC on a day with anaprop. See text for further explanation.

### 3.3 August 19<sup>th</sup>, 1999: Heavy Precipitation

During 18-19 August the synoptic situation 12 UTC shown in figure 3.14 is dominated by a high pressure area with more than 1000 hPa and a northeast gradient with wind from south to southeast. The area got widespread and partly heavy convective precipitation, at places quite huge amounts.

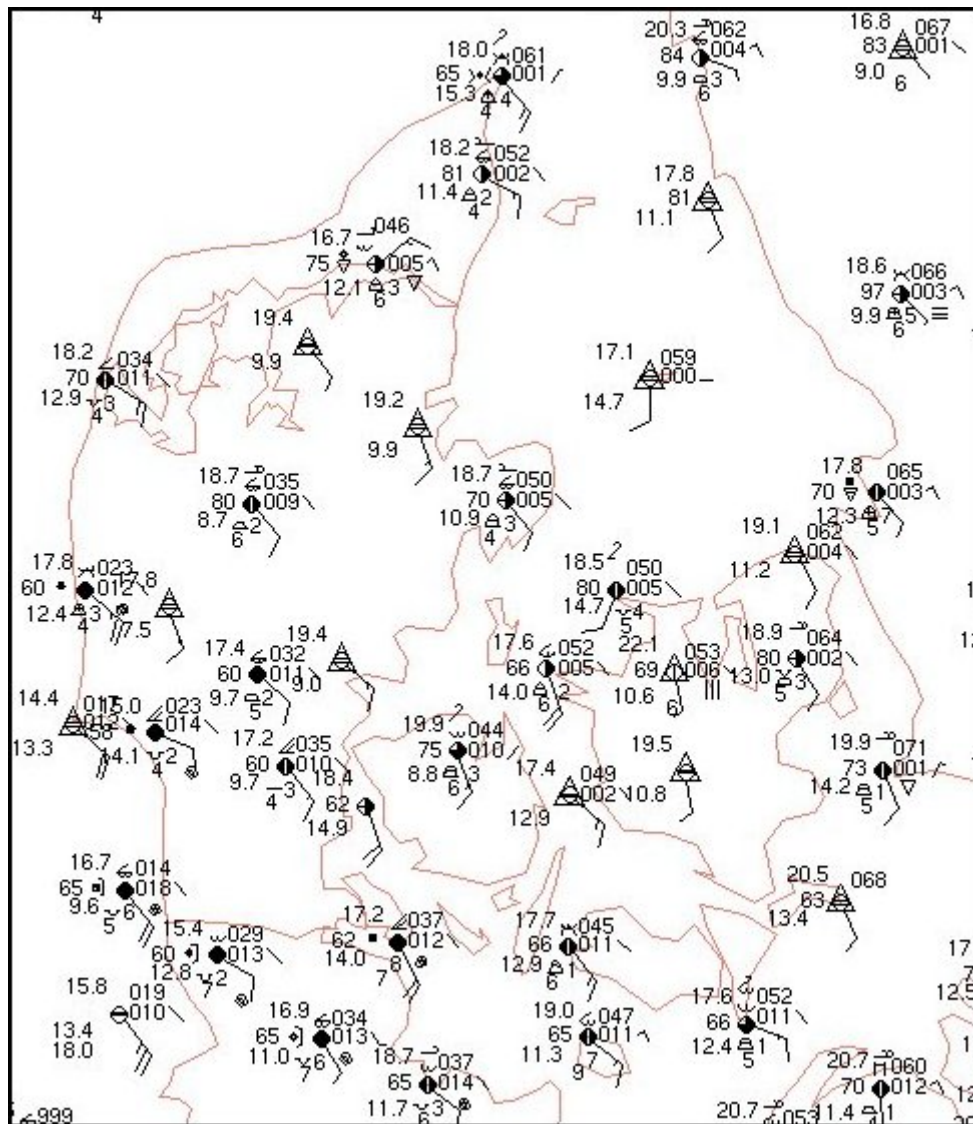


Figure 3.14. Synoptic map for August, 19<sup>th</sup> 1999, 12 UTC.

As shown by the radar images in figure 3.17, the precipitation was at the same time both widespread at some places and very isolated at others in form of smaller heavy showers.

According to climate grid precipitation there were several precipitation maxima with up to about 30 mm of rain as seen in figure 3.15 showing the precipitation contours (red curves) for the radar derived field together with the contours (blue) of the verifying Climate Grid - Denmark and again a scattergram in the lower left corner. There are marked differences in the AMIS, shown in figure 3.16 and radar grid results. Generally, AMIS has difficulties in locating the maximum precipitation correctly. Moreover, the precipitation amounts are very wrong and there are large discrepancies between climate grid and AMIS which can also be seen in the scattergram. Opposite to this, the radar has generally got hold of the position of the large precipitation amounts. Also, it has determined areas with relatively small amounts fairly good. The scattergram in figure 3.15 shows the expected scatter between radar and

climate grid cells, but the spread around the identity line looks like a cone structure pointing towards the intersection between the x- and y-axis.

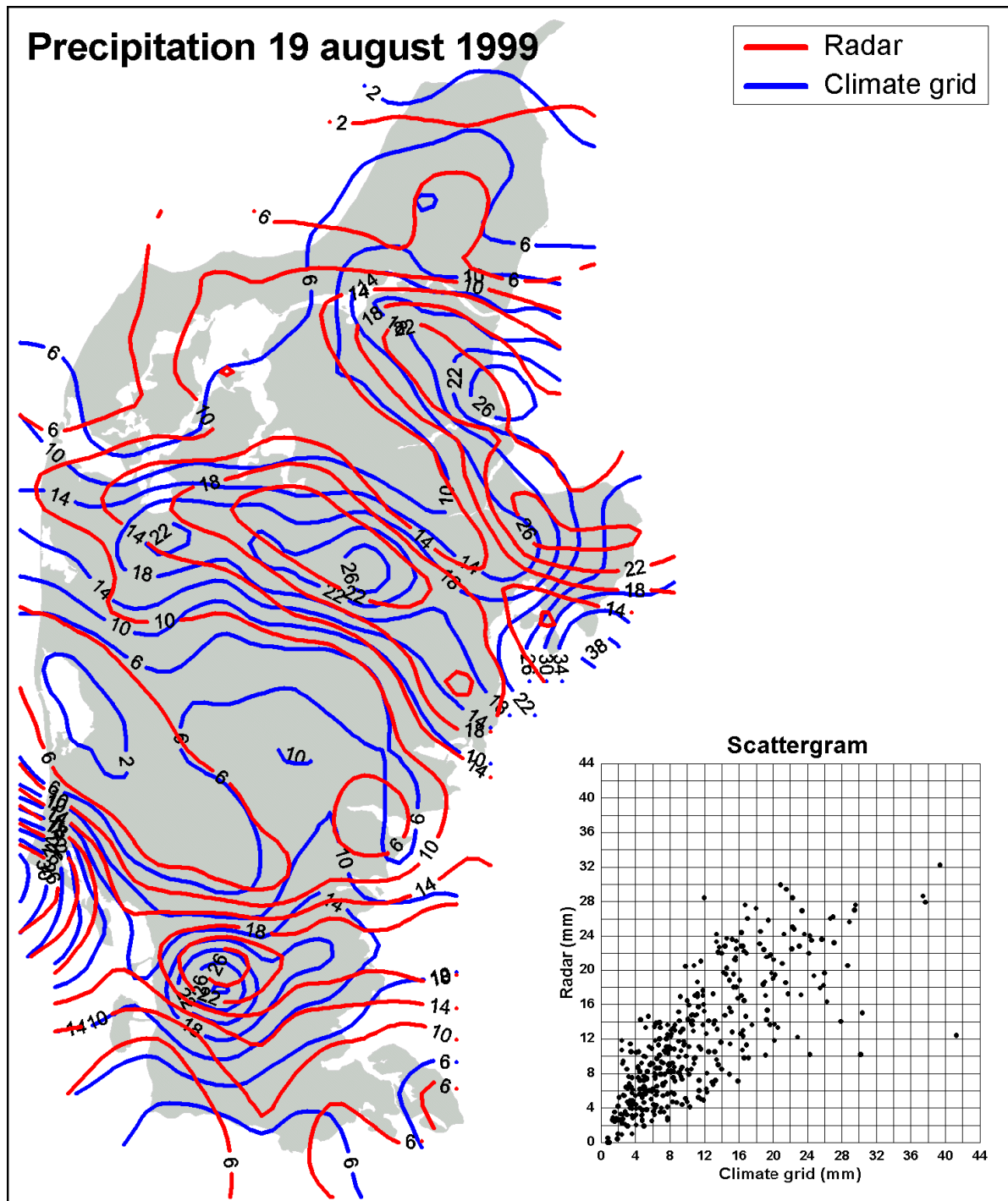


Figure 3.15. Map of precipitation using RADAR for August 19<sup>th</sup> 1999, 12 UTC, and a scattergram to show the accuracy.

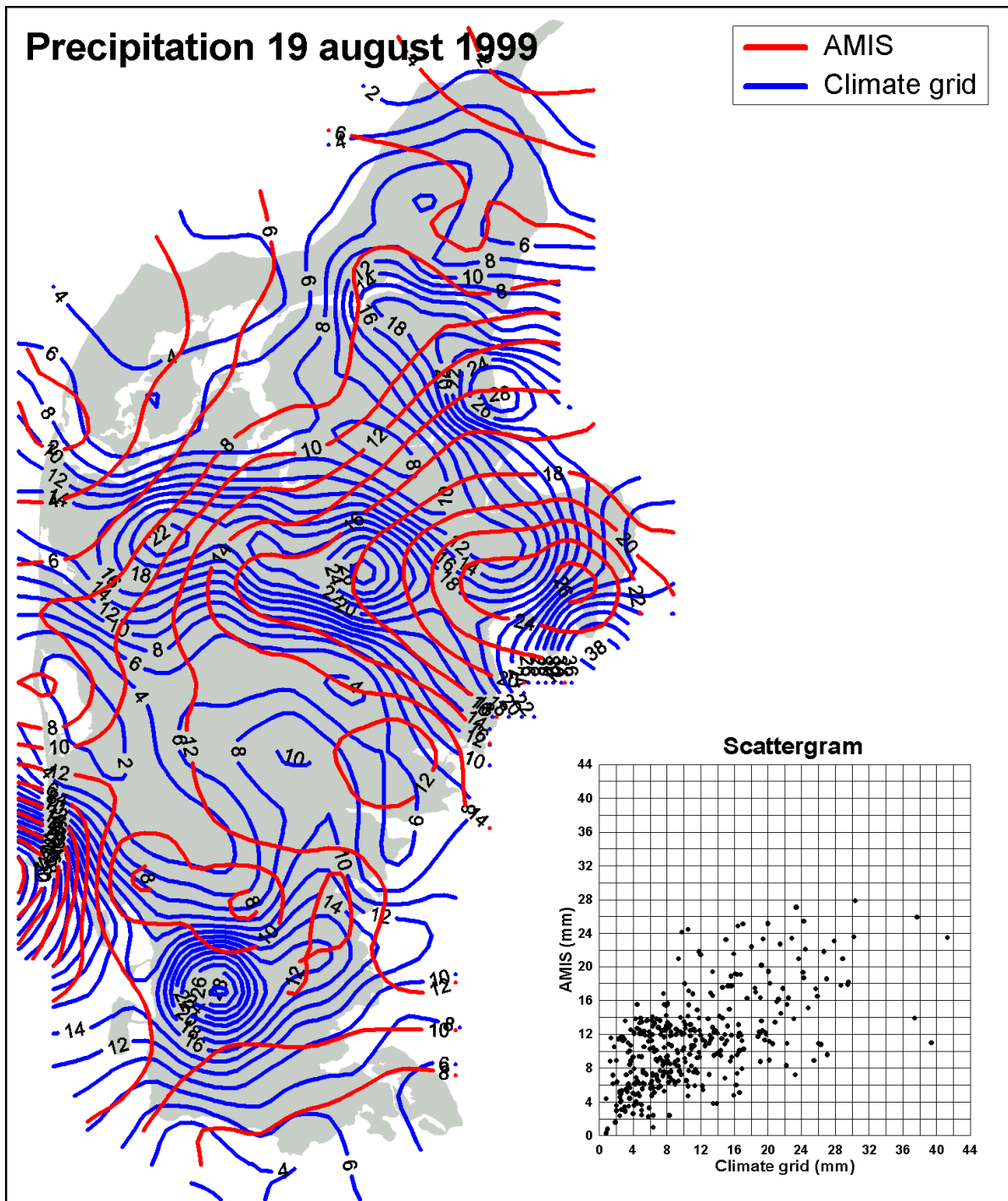


Figure 3.16. Map of precipitation using AMIS for August 19<sup>th</sup> 1999, 12 UTC, and a scattergram to show the accuracy.

Figure 3.17, that shows Rømø and Sindal radar images at 6 UTC, is an illustrative example of what effect widespread and heavy precipitation can have on the detection capability of a weather radar. C-band radars are generally sufficient for monitoring moderate precipitation events, but for monitoring of heavy storms there would probably be no energy left in the radar beam for detection of hydrometeors from the far side of the storm. In the Sindal image in figure 3.17 it is seen that the southern edge of the rain area appear rather ambiguous, an edge that in the Rømø image is very distinct and with much higher echo intensities.

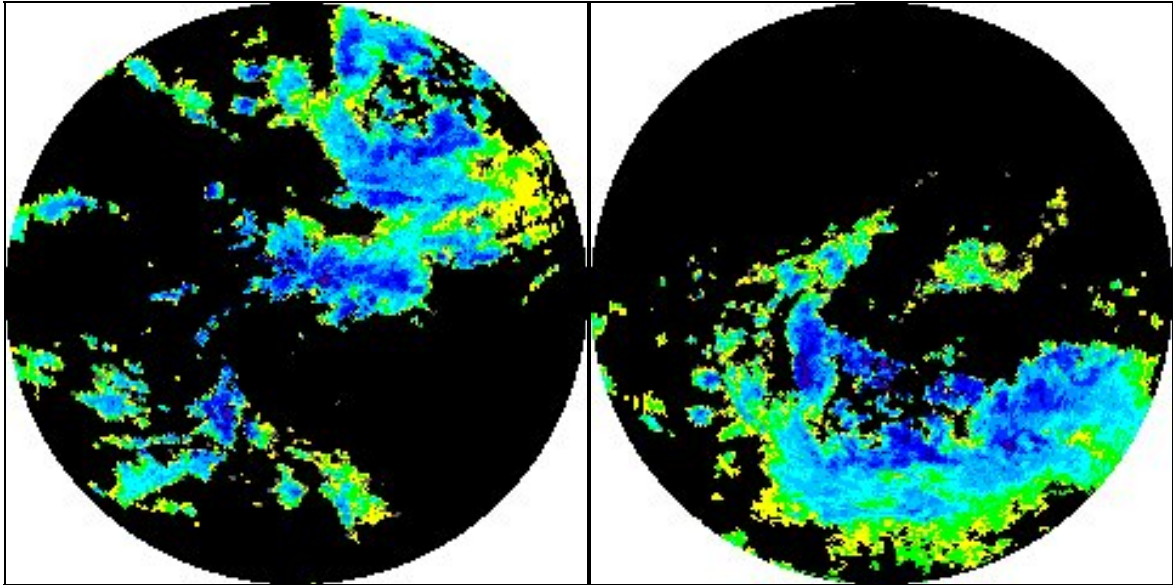


Figure 3.17. Radar images from Rømø (left) and Sindal (right) on August 19<sup>th</sup> 1999 at 6 UTC. Dark blue indicates the heaviest rain, yellow and grey is the weakest.

### 3.4 Conclusions

The main conclusion drawn from the case studies is that the radar derived field generally captures the precipitation patterns much better than the operational AMIS field, especially August 19<sup>th</sup> 1999, where large differences in precipitation across Jutland occurred. This is due to the much denser data coverage provided by the radars. The estimation of the precipitation amounts shows to some extent less scatter for the radar derived precipitation than for the AMIS.

The conclusion based on the case studies thus suggests that the AMIS 24 hour accumulated precipitation would be improved by the inclusion of the radar derived precipitation.

## 4. Verification

### 4.1 Data

The objective verification has been done for the two growing seasons separately, i. e. for April 1 to September 30 1998 and for April 1 to September 30 1999. For both the radar derived 24 hour accumulated precipitation and the AMIS 24 hour accumulated precipitation the field data has been further stratified according to month. Result are presented for each month and for the growing season for both years.

Over the growth seasons in 1998 and 1999 the most of the expected data have been received from the radar in Rømø and Sindal as seen in table 4.1, but there have been periods with problems in data transmission or, most often, data archive difficulties resulting in a not complete storage of received data. At present, these problems have been solved and practically all data are stored in the archive.

For the estimation to be carried it was a basic requirement that only one radar image was allowed to be missing every second hour, i.e. not more than 12 images per day. The number of expected radar images from each radar site is 144 images every 24 hours, i.e. the frequency of data receipt is 10 minutes.

On average, 142 to 144 images was received from both radar sites on days where estimation was possible due to receipt of the required amount of data, and on approximately 85% of the days in the growth season the two years the data requirement was fulfilled. Of these days, up to about 97% of the days had 140 images or more, which is very good.

On the case 15 July 1998, 99.3% of the expected data from the Sindal and Rømø radar have been stored in the data archive. On 25 June 1999 there was no interruptions in the data storage at all, and, finally, on 19 August 1999 a percentage of 99.3% and 97.9% of the expected data from Rømø and Sindal, respectively, have been stored.

<i>Statistics on the amount of expected data that were received</i>	Rømø			Sindal			Sindal and Rømø		
	1998	1999	total	1998	1999	total	1998	1999	total
Number of days with enough data	160	146	306	169	148	317	329	294	623
In pct of total number of days	87.0	79.3	83.2	91.8	80.4	86.1	89.4	79.9	84.6
Number of days with too few data	24	38	62	15	36	51	39	74	113
In pct of total number of days	13.0	20.7	16.8	8.2	19.6	13.9	10.6	20.1	15.4
Average number of images pr. day	143.5	142.4	143.0	141.0	143.7	142.3	142.2	143.1	142.6
Pct. days with $\geq 140$ images	96.9	91.8	94.4	63.9	93.9	77.9	79.9	92.9	86.0

Table 4.1. Statistics on the amount of data received from the radar sites. See text for explanation

## 4.2 Verification Methods

Both data fields are verified against the Climate Grid - Denmark. For each matched grid point the mean error (ME), the mean absolute error (MAE) and the root mean square error (RMSE) is calculated on monthly basis.

Contingency tables with categories 0-0.05, 0.05-2, 2-6, 6-10 and 10-100 mm precipitation/24hr for both fields has been constructed. The contingency tables for the growing seasons are presented below. The contingency tables for each month are placed in appendices C to F. Based on the contingency tables the hit rate (HR) and Hansson Kuipers skill index (HKSI) are calculated for each grid point for every month in the growing seasons.

The maximum, the mean and the minimum value of the ME, MAE and HKSI values of all the grid points covering Jutland are presented in a graphical form for each month and the whole growing season. Tables of all the verification parameters are placed in appendix B.

## 4.3 Results

### 4.3.1 1998

Table 4.2 shows the contingency tables for both the AMIS and the radar derived precipitation fields for the whole growing seasons for the year 1998 .

Climate		0	0,05	2	6	10
Radar		0,05	2	6	10	100
0	0,05	21684	9019	1350	189	13
0,05	2	2734	7104	3577	288	58
2	6	503	1621	4844	1829	635
6	10	159	145	1142	1081	1000
10	100	246	21	244	640	2033

mm

Climate		0	0,05	2	6	10
AMIS		0,05	2	6	10	100
0	0,05	12517	1143	32	1	2
0,05	2	10759	13214	2421	138	38
2	6	249	2073	6586	1503	360
6	10	25	120	1066	1661	947
10	100	19	92	145	513	2319

mm

Table 4.2 Contingency table for April 1<sup>st</sup> 1998 to September 30<sup>th</sup> 1998.

The off diagonal elements for both fields drops quickly except for the radar derived field with only trace precipitation according to climate Grid, where the radar derived field has 246 events with precipitation in the category 10-100 mm/24hr. This is due to anaprop errors, which occur mainly in April (see contingency table for April 1998 appendix E). On the other hand especially trace or very scattered precipitation are captured better by the radar derived field (21684) than the AMIS field (12517).

However the radar derived precipitation field tends to underestimate the amounts of precipitation judged from the larger values in the upper right triangle of the table. Thus days

with larger amounts of precipitation is better represented in the AMIS field. As will be discussed later the radar derived field can probably be improved by a suitable calibration.

Figure 4.1 show curves for the ME, MAE and HKSI verification measures for each month and the whole growing season 1998. The blue curves show the radar derived field and the red curves show the AMIS field. The dotted lines show the minimum values, the thin lines show the maximum values and the thick lines show the mean values.

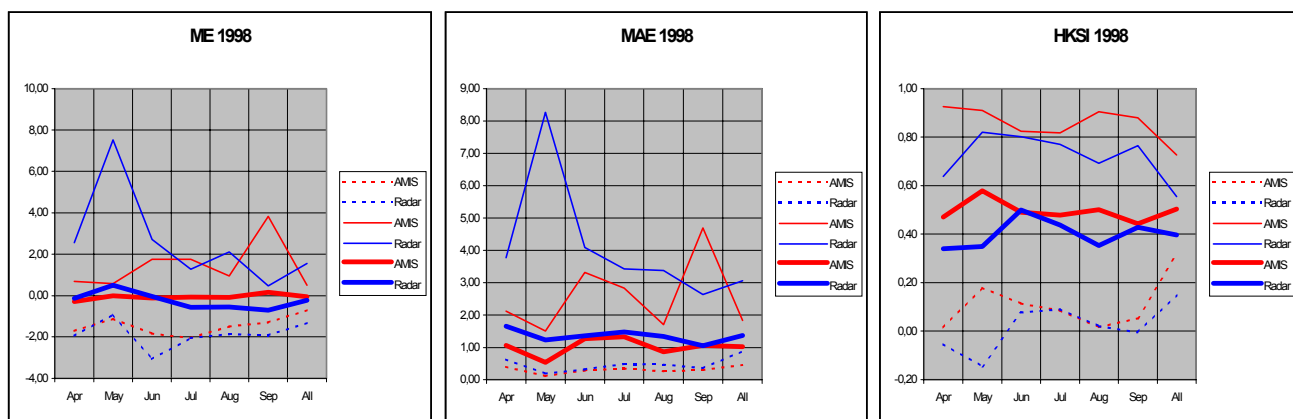


Figure 4.1. Verification measurements for each month of the growing season 1998

The AMIS mean value of the ME is close to zero indicating that AMIS on average is unbiased. This is also nearly true for the radar derived field. The maximum and the minimum ME for the AMIS field are slightly better than the radar derived field values.

The pronounced peak in the radar derived field in May is mainly caused by anaprop May 1<sup>st</sup> due to a temperature surface inversion, resulting in a precipitation estimate of 95 mm/24hr on a total dry day.

The less pronounced peak in the AMIS field in September is due to a reported precipitation amount of 140 mm/12hr September 9<sup>th</sup> at 18:00 UTC at station Bågø (06111).

The two peaks in the ME are also present in the MAE. Furthermore the MAE's for the radar derived field are generally greater than the AMIS values indicating a poorer performance of the radar based system.

The HKSI values for the AMIS field are generally greater than the values for the radar derived field, which further confirms the poorer performance of the radar based system.

### 4.3.2 1999

Table 4.3 shows the contingency tables for both the AMIS and the radar derived precipitation fields for the whole growing seasons for the year 1999.

Also in 1999 the off diagonal elements for both fields drops quickly except for the radar derived field for days with no precipitation (lower left corner value now 597). Again this is due to anaprop errors.

The patterns found for the contingency tables from 1998 are also present in the tables for 1999.

Climate		0	0,05	2	6	10
Radar		0,05	2	6	10	100
0	0,05	18762	4954	488	43	9
0,05	2	3612	4499	2460	357	109
2	6	1117	1186	3565	1748	802
6	10	371	118	828	1300	1092
10	100	597	43	324	686	2267

mm

Climate		0	0,05	2	6	10
AMIS		0,05	2	6	10	100
0	0,05	15454	653	23	4	3
0,05	2	8213	7742	1226	106	54
2	6	284	1893	4892	1127	255
6	10	61	153	1270	1876	839
10	100	41	54	265	1045	3176

mm

Table 4.3 Contingency table for 1/4 1999 to 30/9 1999

Figure 4.2 show curves for the ME, MAE and HKSI verification measures for each month and the whole growing season 1999. Colours and line types are similar to figure 4.1.

Also these verification measures show the same pattern as those of 1998, except that the peaks appear in July in the radar derived field and in September in the AMIS. The peak in the radar derived field is mainly caused by anaprops on July 11<sup>th</sup> and 28<sup>th</sup> due to a temperature surface inversion. The peak in the AMIS field is due to a reported precipitation amount of 34mm/6hr on September 8<sup>th</sup> at 06:00 UTC at station Borriss II (05410).

The mean bias (ME) for the radar derived field is a little bit better in 1999 than in 1998, but else the conclusion drawn from the MAE and the HKSI is the same as for 1998.

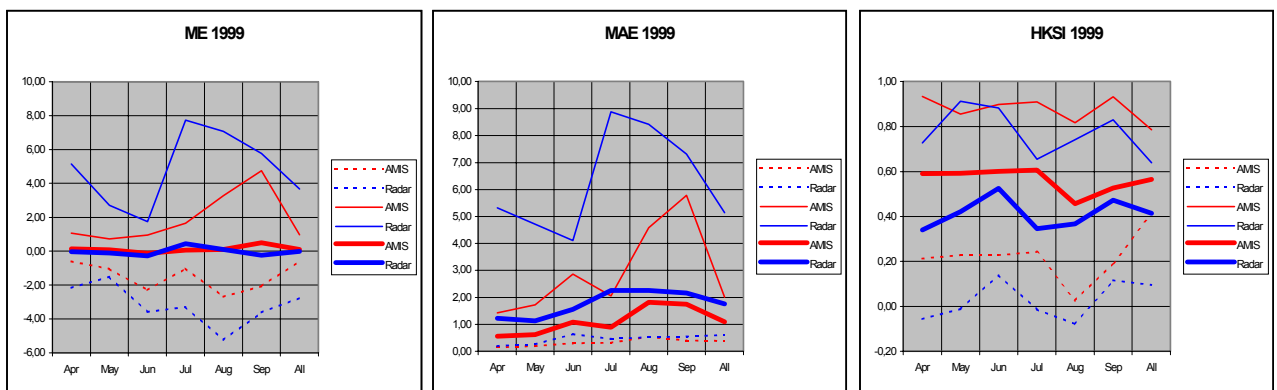


Figure 4.2. Verification measurements for each month of the growing season 1999.

#### **4.4 Conclusions**

The conclusion to be drawn from the overall statistical verification measures is that the inclusion of the radar derived precipitation into the AMIS 24 hour accumulation precipitation would deteriorate the overall statistics of the AMIS.

However this is somewhat contradictory to the conclusion based on the case studies stating that the inclusion of radar derived precipitation would improve the AMIS field. This will be discussed in the final concluding chapter.

## 5. Conclusions and Outlook

For the whole growth season in 1998 and 1999, the verification measures of the radar derived precipitation grid is slightly poorer than that of AMIS. There are some well-founded reasons for this.

First of all, radar data from all ranges and all days with enough radar data in the growth season during the two years have been entered into the evaluation statistics, i.e. the contingency tables and the summing up tables. Consequently, the overall results are affected and contaminated by on beforehand known erroneous radar data such as artificial radar precipitation on dry days which, apparently, can be explained by anaprop or small radar amounts detected at large distances from the radar, where the radar is known to underestimate the rain rate.

The most important sources of error on radar data that can have played a role for the daily results in this study are: beam attenuation, beam power losses at range, clutter, anaprop, bright-band, vertical reflectivity profile variations, beam overshooting and not fulfilled beam filling conditions, i.e. that hydrometeors are not uniformly distributed in the radar bin. In appendix A these errors will be briefly explained.

It must be noticed, that usually these errors do not play the same role from case to case or from one part of the radar image to another. In normal situations, most of the errors in radar data are insignificant for estimation of rain amount, but in special cases certain errors, such as anaprop, can affect the estimations deleteriously. Some of the errors will only occur at large ranges (e.g. vertical reflectivity profile variations and beam overshooting), while other will only affect the estimations in certain seasons (e.g. the bright-band effect) or appear during special weather conditions (anaprop). More or less, these errors have affected the growth season results, but it is impossible to quantify it without doing a detailed inspection of the daily results.

If appropriate corrections were applied, the radar would certainly perform much better. Fortunately, something can be done to correct for all or the most of these errors in order to improve radar estimates of rain rate and precipitation amount.

The anaprop error is assumed to contribute significantly to the evaluation statistics, mainly in those weather situations with no precipitation. These weather situations may be identified by comparison with real time rain gage measurements. This strategy will however not work straight forward in weather situations with both precipitation and anaprop. A method to handle this could be some threshold limit for real time differences from rain gage measurements.

It is therefore recommended that the next project focus on the development and evaluation of correction methods for the anaprop error.

Secondly, a widely used fixed empirical expression of the form  $Z=220R^{1.60}$  has been used in order to calculate the rain rate R from the radar reflectivity factor Z, i.e. by the so-called Marshall-Palmer equation (Marshall and Palmer, 1948). The expression is valid for

widespread frontal rain that is often seen in weather situations in Denmark. The magnitude of the error on the adjustment when using fixed constants in the Z-R equation depends on how much the drop size distribution of the actual rainfall deviates from the drop size distribution assumed in the relationship, thus spatial and temporal variations in rain rate will affect the results. One consequence is, that using a frontal equation on rain shower will result in underestimation of precipitation amount which is seen in the case results.

This argues for an adjustment that is based on a comparison between parallel radar measures and rain gauge recordings, which is recommended as part of the next project.

At last, an error in the calibration of the receiver sensibility in the Rømø radar has subsequently been diagnosed, and the effect of it has been a general underestimation of the precipitation amount and some problems in showing the amount and spatial distribution of precipitation. This has also affected the overall results of the present study.

It must be mentioned, that the receiver problems in the Rømø radar have been solved.

To sum up the radar grid estimates are assumed to be improved by :

1. Applying correction for the anaprop errors on radar data in order to improve radar estimates of rain rate and precipitation amount.
2. Implementing and applying a rain gauge adjustment based on simultaneous radar measures and rain gauge recordings for each individual case.

The overall statistical verification measures of the radar derived precipitation grid was found slightly poorer than that of AMIS in the study. If the above mentioned action points are dealt with, an improvement of the overall performance of the radar would certainly be expected.

Based on the previous discussion and the very promising results from the case studies it may be concluded that the use of radar data will improve the AMIS 24 hour accumulated precipitation beyond its present level.

## 6. References

Austin, P. M. (1987): *Relation between measured Radar Reflectivity and Surface Rainfall*. Mon. Wea. Rev., vol. 115, p. 1053-1070.

Battan, L. J. (1973): *Radar observation of the atmosphere*. The University of Chicago Press, Chicago, p. 1-113 and p. 324.

Collier, C. G. (1989). *Applications of weather radar systems*. Ellis Horwood, pp 294

Scharling, M.: *Climate grid Denmark, Precipitation, air temperature, and potential evaporation 20x20 & 40x40 km, method description*. DMI Technical report 99-12

Scharling, M.: *Climate Grid - Denmark, Precipitation 10\*10 km (Version 2)*. DMI Technical report 99-15

Hanssen, A.W., and W.J.A. Kuipers (1965): *On the relationship between the frequency of rain and various meteorological parameters*. De bilt, KNMI, Mededelingen en Verhandelingen, 81.

Hilden, A. and J. Hansen, 1998: *Quality and availability of AMIS data for the growing seasons of 1997 and 1998*. DMI Technical Report 98-19, DMI 1998

Joss, J. and A. Waldvogel (1987): *Precipitation measurements and hydrology*. 40. ann. Conf. on Radar Meteorology.

Joss, J., G. Galli, G. D. Bruna (1995): *Seven years of (dis-)agreement between radar, rain gauges and river flow: possible improvements?* Prepared for the 27th International Conference on Radar Meteorology 9-13 October 1995 in Vail, Colorado.

Kitchen and Jackson (1993): *Weather radar performance at long range - simulated and observed*. J. Appl. Met., vol. 32, 975-85.

Marshall, J. S. and W. McK. Palmer (1948): *The distribution of raindrops with size*. J. Meteor., vol. 5, 165-166.

Mikkelsen, H.E. & Olesen J.E (1991): "*Sammenligning af metoder til bestemmelse af potentiel vandfordampning*". Landbrugsministeriet, Statens Planteavlfsforsøg, Tidsskrift for Planteavlfs Specialserie, Beretning nr. S 2157).

Smith, P. L. (1990): *Precipitation Measurements and Hydrology: Panel Report. Radar in Meteorology, Battan Memorial and 40th Anniversary Radar Meteorology Conference*, Am. Met. Soc., Boston 1990, 607-618.

Zawadski, I. (1984): *Factors affecting the precision of radar measurements of rain*. 22nd Conference On Radar Meteorology, 10-13. Sept. 1984, Zürich, Switzerland. Publ. Am. Met. Soc., 251-256.

# Appendix A

## **A brief explanation of errors on weather radar data**

In the following, important sources of error on radar data will be briefly explained and discussed.

### *Clutter and anomalous beam propagation (anaprop):*

Clutter which is reflection of the radar beam from ground targets close to the radar is always more or less present in a radar image. In stable weather conditions temperature and vapour inversions may be present causing the radar beam to be refracted more than the curvature of Earth. Therefore, the beam hits ground targets at random radar ranges and artificial precipitation patterns are seen in the image (anaprop).

### *The bright-band effect:*

If melting snow is present at level the reflection of the beam can be enhanced by up to a factor of 5 due to the fact, that the backscatter cross section of the hydrometeor becomes larger because of a coverage of a thin water film on the melting snow. The rain rate is unchanged but the radar echo increases. As noted by Smith (1990) it is not so complicated to recognise a bright-band in stratiform precipitation as it is in convective. For correction of the bright-band effect, the radar must have the necessary spatial resolution to resolve the bright-band layer. This is possible for the Sindal and Rømø radars and the newly installed radar at Stevns.

### *Beam attenuation due to hydrometeors and atmosphere:*

If melting snow, hail or ground clutter is present, incorrect values for attenuation correction will be applied to the bins causing errors in the output (Collier, 1989). For example, the correction for attenuation due to hail is so unreliable that the derived rain rates cannot be used with any confidence, because for a C band radar, dry hail causes large reflectivities but smaller attenuation than rain. However, if hail less than some specific diameter is coated with a thin film of water the attenuation increases (Battan, 1973).

### *Beam power losses at range and beam filling conditions*

At increasing range the volume of the polar bin increases. The spatial distance between the Polar bins increases with range and the resampling becomes more inaccurate at longer range. At range beam filling conditions may not be fulfilled and, together with small scale variability of precipitation, the radar echo may not be representative of the precipitation conditions within the distant Polar bins. The radar measures the meteorological targets within a volume at a certain altitude above the ground surface. The problem increases with range, and for example, beam filling combined with reduced visibility can play an important role at longer ranges (Joss et al., 1995).

A rule of thumb is that closer to the radar than 100-150 km data can be used quantitatively, but at large ranges it can most often only be used qualitatively unless data are corrected for range related sources of error which can improve results to a certain extent.

### *Vertical reflectivity profile variations and beam overshooting*

At increasing range from the radar, the vertical distance between the sampling volume and the ground surface usually increases, and serious errors may arise from the variations in the vertical reflectivity profile. For example, below the radar beam the rain rate may change due to low level evaporation in a dry atmosphere, low growth in a moist atmosphere or orographic growth due to local terrain effects.

At long range, overshooting of the radar beam can cause no detection of precipitation areas, but also, missing radar samples at low altitudes may lead to a strongly underestimated rain rate. The overshooting problem is especially important in winter where the vertical extent of snowfall echoes are often less than 2 km above the ground.

When the radar beam is passing near the top of the precipitation layer the reflectivity fluctuations are not well correlated with the changes in the rain rate near the ground. In fact, Kitchen and Jackson (1993) discussed that the underestimation of rainfall accumulations at longer ranges (>100 km) is mainly caused by a steep decline in probability of detection, i.e. detection failure, and not so much by underestimation of the precipitation rate.

### *Rain gauge adjustment*

Following Joss and Waldvogel (1987) that corrections for all known systematic errors on radar data should be applied before any rain gauge adjustment. And really, something can be done to nearly all, and at least to the most important errors. On the other hand, raingauge adjustment must be done carefully because of the different nature of radar and raingauge measurements; radar data are an instant volume measure and rain gauging is a point measure of accumulated precipitation. The representativity problem can affect the comparison and has to be considered. Statistical methods for comparison can to some extent eliminate, or at least reduce, the effect of this problem.

In order to use radar for measuring rainfall intensity  $R$ , most investigators have employed an empirical expression of the general form  $Z=AR^b$  where  $A$  and  $b$  are constants. The relationship between  $Z$  and  $R$  is affected by various physical processes. Spatial and temporal variations of rain rate will affect the radar and rain gauge samples differently, and, unless treated, it will affect the raingauge adjustment. By experience it is known that the effect of not representative samples can be reduced by using many  $Z$ - $R$  values in the same rainfall system (Austin, 1987), but on the other hand many samples do not remove the scatter of the individual samples (Zawadski, 1984).

### *Variations in the drop size distribution*

The rain gauge measurements are affected by the aerodynamic error and shelter effect and, if the wind speed is high, it must be dealt with before rain gauge adjustment. The magnitude of the error on the adjustment when fixed constants in the  $Z$ - $R$  equation is used depends on how much the drop size distribution of the actual rainfall deviates from the drop size distribution assumed in the equation. In this pilot study it is the Marshall and Palmers equation, thus spatial and temporal variations in rain rate can affect the results. This argues for an adjustment based on parallel rain gauge and radar measures.

## Appendix B Tables with the overall statistics for 1998 and 1999

The verifications parameters are calculated for each of the grid point covering Jutland on monthly basis.

Monthly minimum, maximum values of all the grid points are presented below together with the the monthly average values over all grid points covering Jutland. Minimum, maximum and average values for the whole growing season is also presented.

			ME		MAE		RMSE		HR		HKSI	
			Radar	AMIS	Radar	AMIS	Radar	AMIS	Radar	AMIS	Radar	AMIS
1 9 9 8	M I N	Apr	-1,94	-1,70	0,63	0,40	0,97	0,65	0,23	0,22	-0,05	0,02
		May	-0,92	-1,13	0,19	0,12	0,38	0,24	0,19	0,45	-0,14	0,18
		Jun	-3,08	-1,84	0,32	0,29	0,58	0,60	0,33	0,33	0,08	0,11
		Jul	-2,05	-2,06	0,49	0,34	0,78	0,55	0,30	0,30	0,09	0,09
		Aug	-1,87	-1,49	0,47	0,26	0,81	0,38	0,27	0,27	0,02	0,02
		Sep	-1,92	-1,30	0,36	0,30	0,60	0,42	0,29	0,25	0,00	0,05
		All	-1,33	-0,71	0,88	0,46	1,62	0,93	0,45	0,48	0,15	0,32
	M A X	Apr	2,56	0,70	3,78	2,12	8,57	5,26	0,73	0,96	0,64	0,93
		May	7,53	0,57	8,26	1,50	22,31	3,84	0,94	0,93	0,82	0,91
		Jun	2,72	1,75	4,09	3,33	14,25	7,62	0,85	0,89	0,80	0,82
		Jul	1,26	1,74	3,43	2,84	6,24	6,75	0,83	0,87	0,77	0,82
		Aug	2,10	0,96	3,37	1,70	9,71	3,69	0,81	0,92	0,69	0,90
		Sep	0,47	3,82	2,64	4,70	5,93	18,98	0,88	0,88	0,76	0,88
		All	1,55	0,50	3,06	1,83	10,37	7,50	0,71	0,80	0,55	0,73
	M E A N	Apr	-0,14	-0,29	1,66	1,07	3,08	1,95	0,51	0,62	0,34	0,47
		May	0,50	-0,01	1,23	0,54	3,00	1,27	0,62	0,71	0,35	0,58
		Jun	-0,05	-0,11	1,36	1,27	2,98	2,60	0,65	0,61	0,50	0,49
		Jul	-0,57	-0,07	1,48	1,33	2,73	2,49	0,58	0,61	0,44	0,48
		Aug	-0,55	-0,09	1,35	0,87	2,69	1,61	0,56	0,63	0,35	0,50
		Sep	-0,72	0,16	1,05	1,06	2,09	2,23	0,64	0,56	0,43	0,44
		All	-0,23	-0,07	1,36	1,02	3,07	2,24	0,59	0,63	0,40	0,50

			ME		MAE		RMSE		HR		HKSI	
			Radar	AMIS	Radar	AMIS	Radar	AMIS	Radar	AMIS	Radar	AMIS
1 9 9 9	M I N	Apr	-2,16	-0,60	0,20	0,14	0,36	0,23	0,29	0,43	-0,06	0,21
		May	-1,51	-1,05	0,26	0,20	0,48	0,31	0,28	0,40	-0,01	0,23
		Jun	-3,60	-2,30	0,64	0,30	1,03	0,49	0,38	0,40	0,14	0,23
		Jul	-3,29	-1,02	0,46	0,32	0,91	0,60	0,19	0,46	-0,01	0,24
		Aug	-5,25	-2,69	0,52	0,54	0,84	1,06	0,19	0,24	-0,08	0,03
		Sep	-3,61	-2,07	0,54	0,40	1,04	0,78	0,29	0,33	0,12	0,19
		All	-2,77	-0,61	0,61	0,38	1,24	0,73	0,37	0,51	0,09	0,41
	M A X	Apr	5,15	1,06	5,32	1,42	18,05	2,39	0,86	0,95	0,73	0,93
		May	2,70	0,73	4,72	1,73	10,30	6,30	0,96	0,88	0,91	0,86
		Jun	1,75	0,95	4,11	2,87	9,60	7,90	0,92	0,92	0,88	0,90
		Jul	7,73	1,66	8,88	2,05	22,54	5,74	0,77	0,92	0,65	0,91
		Aug	7,07	3,27	8,41	4,58	20,69	15,62	0,82	0,86	0,74	0,82
		Sep	5,77	4,74	7,31	5,78	13,45	11,53	0,86	0,95	0,83	0,93
		All	3,68	0,96	5,13	2,01	12,87	6,72	0,78	0,83	0,64	0,79
	M E A N	Apr	-0,03	0,13	1,22	0,55	2,71	1,04	0,58	0,68	0,34	0,59
		May	-0,11	0,07	1,13	0,63	2,53	1,30	0,64	0,68	0,42	0,59
		Jun	-0,28	-0,12	1,55	1,08	2,90	2,04	0,65	0,67	0,53	0,60
		Jul	0,43	0,06	2,25	0,89	4,87	1,92	0,54	0,71	0,35	0,61
		Aug	0,09	0,10	2,26	1,81	4,36	3,50	0,53	0,57	0,37	0,46
		Sep	-0,23	0,49	2,16	1,74	3,95	2,94	0,61	0,59	0,47	0,53
		All	-0,01	0,11	1,76	1,09	3,95	2,40	0,59	0,65	0,41	0,57

## Appendix C Contingency tables for AMIS for each month in the growing season 1998

Climate		0	0,05	2	6	10
AMIS		0,05	2	6	10	100
0	0,05	715	227	1	1	0
0,05	2	1437	2265	448	22	4
2	6	10	354	1667	360	27
6	10	0	3	105	229	130
10	100	0	0	3	40	347

mm

Contingency table for 1/4-98 - 30/4-98

Climate		0	0,05	2	6	10
AMIS		0,05	2	6	10	100
0	0,05	4965	251	7	0	2
0,05	2	1722	1520	278	34	10
2	6	52	283	706	186	31
6	10	1	11	134	181	63
10	100	0	2	14	27	65

mm

Contingency table for 1/5-98 - 31/5-98

Climate		0	0,05	2	6	10
AMIS		0,05	2	6	10	100
0	0,05	2279	176	6	0	0
0,05	2	1712	2290	457	31	20
2	6	101	387	839	342	99
6	10	21	36	120	171	108
10	100	4	40	50	88	466

mm

Contingency table for 1/6-98 - 30/6-98

Climate		0	0,05	2	6	10
AMIS		0,05	2	6	10	100
0	0,05	1188	161	1	0	0
0,05	2	1641	2899	520	17	3
2	6	17	528	1476	300	123
6	10	0	30	410	548	237
10	100	15	22	38	152	595

mm

Contingency table for 1/7-98 - 31/7-98

Climate		0	0,05	2	6	10
AMIS		0,05	2	6	10	100
0	0,05	1605	117	7	0	0
0,05	2	2058	2755	407	21	0
2	6	50	202	892	132	36
6	10	0	11	142	278	201
10	100	0	2	25	77	470

mm

Contingency table for 1/8-98 - 31/8-98

Climate		0	0,05	2	6	10
AMIS		0,05	2	6	10	100
0	0,05	1765	211	10	0	0
0,05	2	2189	1485	311	13	1
2	6	19	319	1006	183	44
6	10	3	29	155	254	208
10	100	0	26	15	129	376

mm

Contingency table for 1/9-98 - 30/9-98

## Appendix D Contingency tables for AMIS for each month in the growing season 1999

Climate		0	0,05	2	6	10
AMIS		0,05	2	6	10	100
0	0,05	2273	55	0	0	0
0,05	2	1596	1670	98	1	0
2	6	8	238	884	143	14
6	10	0	12	160	228	80
10	100	0	0	5	72	128

mm

Contingency table for 1/4-99 - 30/4-99

Climate		0	0,05	2	6	10
AMIS		0,05	2	6	10	100
0	0,05	2858	33	0	0	0
0,05	2	1841	1709	164	4	0
2	6	1	469	1067	140	10
6	10	0	1	95	249	107
10	100	0	0	1	69	298

mm

Contingency table for 1/5-99 - 31/5-99

Climate		0	0,05	2	6	10
AMIS		0,05	2	6	10	100
0	0,05	2538	117	6	3	0
0,05	2	1159	1209	211	22	14
2	6	10	350	1090	357	57
6	10	0	1	212	503	221
10	100	0	0	13	219	812

mm

Contingency table for 1/6-99 - 30/6-99

Climate		0	0,05	2	6	10
AMIS		0,05	2	6	10	100
0	0,05	3634	162	1	0	0
0,05	2	1152	1708	375	22	11
2	6	4	311	815	143	34
6	10	0	45	206	192	119
10	100	0	7	35	143	361

mm

Contingency table for 1/7-99 - 31/7-99

Climate		0	0,05	2	6	10
AMIS		0,05	2	6	10	100
0	0,05	2109	259	16	1	3
0,05	2	1109	867	274	49	25
2	6	44	352	543	170	90
6	10	5	67	244	302	165
10	100	0	34	129	221	582

mm

Contingency table for 1/8-99 - 31/8-99

Climate		0	0,05	2	6	10
AMIS		0,05	2	6	10	100
0	0,05	2042	27	0	0	0
0,05	2	1356	579	104	8	4
2	6	217	173	493	174	50
6	10	56	27	353	402	147
10	100	41	13	82	321	995

mm

Contingency table for 1/9-99 - 30/9-99

## Appendix E Contingency tables for Radar for each month in the growing season 1998

Climate		0	0,05	2	6	10
Radar		0,05	2	6	10	100
0	0,05	2898	2131	827	149	10
0,05	2	186	1144	602	49	1
2	6	13	437	989	185	29
6	10	1	38	411	197	89
10	100	1	4	93	221	395

mm

Contingency table for 1/4-98 - 30/4-98

Climate		0	0,05	2	6	10
Radar		0,05	2	6	10	100
0	0,05	5495	1105	166	12	3
0,05	2	1248	975	419	22	8
2	6	297	167	437	142	31
6	10	101	21	193	115	46
10	100	178	5	40	152	92

mm

Contingency table for 1/5-98 - 31/5-98

Climate		0	0,05	2	6	10
Radar		0,05	2	6	10	100
0	0,05	3696	1139	92	4	0
0,05	2	395	1462	396	32	7
2	6	65	330	741	277	91
6	10	16	33	211	244	202
10	100	21	4	46	85	400

mm

Contingency table for 1/6-98 - 30/6-98

Climate		0	0,05	2	6	10
Radar		0,05	2	6	10	100
0	0,05	2562	1561	76	6	0
0,05	2	314	1738	856	109	13
2	6	31	356	1315	566	157
6	10	7	21	205	273	251
10	100	2	8	35	81	557

mm

Contingency table for 1/7-98 - 31/7-98

Climate		0	0,05	2	6	10
Radar		0,05	2	6	10	100
0	0,05	3135	1733	51	5	0
0,05	2	481	1143	688	42	24
2	6	83	215	692	342	196
6	10	31	31	50	85	178
10	100	41	0	11	45	318

mm

Contingency table for 1/8-98 - 31/8-98

Climate		0	0,05	2	6	10
Radar		0,05	2	6	10	100
0	0,05	3898	1350	138	13	0
0,05	2	110	642	616	34	5
2	6	14	116	670	317	131
6	10	3	1	72	167	234
10	100	3	0	19	56	271

mm

Contingency table for 1/9-98 - 30/9-98

# Appendix F Contingency tables for Radar for each month in the growing season 1999

Climate		0	0,05	2	6	10
RADAR		0,05	2	6	10	100
0	0,05	3087	1109	169	8	0
0,05	2	576	763	329	63	2
2	6	156	123	530	198	98
6	10	43	1	122	114	76
10	100	71	0	14	66	52

mm

Contingency table for 1/4-99 - 30/4-99

Climate		0	0,05	2	6	10
RADAR		0,05	2	6	10	100
0	0,05	4115	1125	97	2	0
0,05	2	493	923	539	29	1
2	6	88	172	554	254	71
6	10	43	10	63	132	126
10	100	43	3	89	55	223

mm

Contingency table for 1/5-99 - 31/5-99

Climate		0	0,05	2	6	10
RADAR		0,05	2	6	10	100
0	0,05	3342	487	15	5	3
0,05	2	357	848	363	54	14
2	6	54	328	735	452	190
6	10	7	19	220	337	285
10	100	3	2	64	187	509

mm

Contingency table for 1/6-99 - 30/6-99

Climate		0	0,05	2	6	10
RADAR		0,05	2	6	10	100
0	0,05	3194	927	108	12	3
0,05	2	880	896	468	55	21
2	6	362	349	705	216	136
6	10	140	72	138	155	152
10	100	289	17	37	67	220

mm

Contingency table for 1/7-99 - 31/7-99

Climate		0	0,05	2	6	10
RADAR		0,05	2	6	10	100
0	0,05	2205	862	66	3	1
0,05	2	659	748	462	73	31
2	6	272	152	518	260	153
6	10	94	13	158	268	188
10	100	126	20	55	155	506

mm

Contingency table for 1/8-99 - 31/8-99

Climate		0	0,05	2	6	10
RADAR		0,05	2	6	10	100
0	0,05	2819	444	33	13	2
0,05	2	647	321	299	83	40
2	6	185	62	523	368	154
6	10	44	3	127	294	265
10	100	65	1	65	156	757

mm

Contingency table for 1/9-99 - 30/9-99

